Tunable Open-Access Microcavities for Solid-State Quantum Photonics and Polaritonics

Feng Li, Yiming Li, Yin Cai, Peng Li, Haijun Tang, and Yanpeng Zhang*

Optical microcavities are powerful platforms widely applied in quantum information and integrated photonic circuits, among which the open-access microcavity is a newly emerging cavity structure consisting of a micro-sized concave mirror and a planar mirror controlled individually by groups of nanopositioners, whilst light emitters can be grown or transferred at the antinode of the cavity optical modes. Compared with monolithic microcavities, the open-access microcavity enables the simultaneous realization of small mode volume, large-range tunability, flexible structural engineering, and easiness for integration with external emitters, exhibiting extensive applications in the fields of solid-state quantum photonics and polaritonics over the last decade. This review first introduces the basic theory and the construction methods of open-access microcavities, followed by the recent advances of their applications in exciton-polaritons, photon condensates, quantum light sources, and nanoparticle sensing.

1. Introduction

Optical microcavities are solid-state systems confining light to a scale of micrometers via highly reflecting faces or successive total internal reflections, used as indispensable tools for tailoring the temporal and spatial profiles of confined photons.[1] In the time or frequency domain, the confinement determines the boundary conditions for electromagnetic waves, resulting in a series of cavity modes distributed at discrete optical frequencies. Photons of these frequencies experience long lifetime before escaping from the microcavity, characterized by the cavity quality factor Q. In the space or momentum domain, spatial mode profile forms, featured by the mode volume V, and the corresponding photon momentum distribution of the mode determines the far-field profile. The photon density of states inside the cavity, which is proportional to Q/V, quantifies how strong the cavity photon can potentially interact with a given emitter. If the interacting energy between the emitter and the cavity photon exceed their own dissipation rates, the emitter-in-cavity system enters the strong coupling regime in which new eigenstates named cavity polaritons occur, exhibiting a mixed feature of light and matter.[2,3] Otherwise, the system stays in the weak coupling regime in which the emitter and cavity lifetimes are modified by each other, resulting in cavity-enhanced or cavity-prohibited spontaneous emission, known as the Purcell effect.[4,5]

Microcavities play a significant role in a wide range of research areas including light–matter interaction,[2] nonlinear optics,[6] quantum information,[7] and topological photonics,[8,9] serving as crucial elements of on-chip microlasers,[10] optical switches,[11] isolators,[12,13] sensors,[14] photonic logic gates,[15] quantum simulators,[16,17] and high-efficiency quantum light sources.[18] The main advantage of the microcavities over the macroscopic cavities is the small mode volume that is a necessity for enhancing light–matter interaction. On the other hand, the monolithic structure of most microcavities, including Fabry–Perot (FP) cavities, whispering-gallery mode (WGM) cavities, photonic crystals, makes them lack the capability of large-range spectral and spatial tuning, which is, nevertheless, easily accessible by macroscopic cavities which contain separated adjustable cavity mirrors.

Open-access microcavities are designed to combine the advantages of both: large range of tunability and small mode volume. The cavity consists of a planar mirror and a microscale concave mirror coated with either metal or distributed Bragg reflectors (DBR) which are highly reflective and facing each other with a micron-sized gap (illustrated in **Figure 1**b), whilst their relative positions can be tuned individually by nanopositioners. The two mirrors can therefore be separated to make the cavity "open-access" for embedding emitters or engineering inner geometries. This type of design is essential for a broad range of applications in high-quality quantum light sources and exciton-polariton-based devices. For quantum light sources, the open-access microcavity not only allows in situ tunability of the cavity position to hold the nanoscale quantum emitter at the very center of the optical field maximum, but also allows in situ spectral tunability to achieve perfect resonance in frequency between the quantum emitter transition and the cavity mode. This is significant for enhancing

Prof. F. Li, Y. Li, Dr. Y. Cai, P. Li, H. Tang, Prof. Y. Zhang
Key Laboratory for Physical Electronics and Devices of the Ministry of Education & Shaanxi
Key Lab of Information Photonic Technique
School of Electronic and Information Engineering
Xi'an Jiaotong University
Xi'an 710049, P. R. China
E-mail: felix831204@xjtu.edu.cn
Dr. F. Li
Department of Physics and Astronomy
University of Sheffield
Sheffield S3 7RH, UK

The ORCID identification number(s) for the author(s) of this article can be found under https://doi.org/10.1002/qute.201900060

DOI: 10.1002/qute.201900060

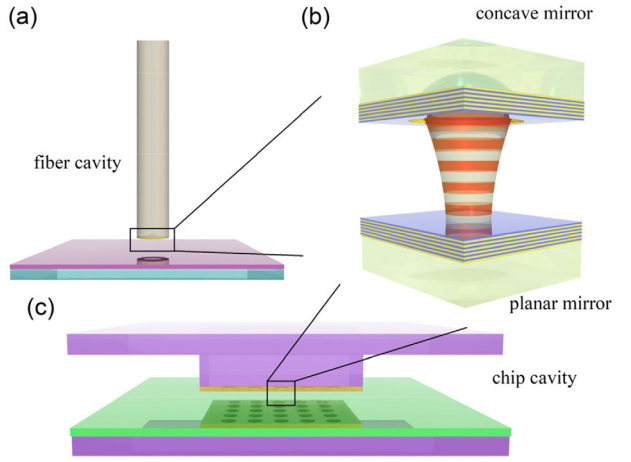

Figure 1. Schematics of open-access microcavities. a) Fiber-based microcavity. b) Enlarged view of the cavity structure. The confined Gaussian modes supported by the planar-concave cavity structure is drawn with optical nodes and antinodes. c) Chip-based microcavity arrays.

optical collection efficiency and emission rate, therefore crucial for the brightness of the quantum light source. For exciton-polaritons, the open-access microcavity provides strong 3D optical confinement without requiring etching into the active media. This allows enhancing the nonlinear polariton–polariton interaction while keeping long coherence time of exciton-polaritons, promising to realize quantum simulators with few strongly interacting polaritons. In addition, the open-access microcavity allows versatile in-cavity engineering of the spatial and spinor properties of polaritons, with potential application to control polariton fluids on photonic chips.

Another unique merit of the open-access microcavity is its easy integration with external light emitters, such as transition metal dichalcogenide (TMD) monolayers, vacancy centers in diamonds, organic semiconductors and nanoparticles. These emitters are difficult to be integrated into high-quality monolithic microcavities due to technical obstacles of depositing high-quality DBR on top, whilst open-access microcavities do not involve such problems and offer a versatile platform for studying light–matter interaction with flexible choice of optical materials.

The review is structured as follows: Section 2 introduces the construction of open-access microcavities, including the basic theory of mode profiles, fabrication methodology, and structure setup. Section 3 reports the recent advances of exciton-polaritons and photon condensates in open-access microcavities. Section 4 reports the recent advances in the applications of open-access microcavities on quantum emitters and nanoparticle sensing. Section 5 summarizes the review and provides outlooks.

Feng Li received the bachelor and master degrees from Tianjin University in China in 2006 and 2008, and a Ph.D. in Physics at Université Nice Sophia-Antipolis in France in 2013 based on the research activities at CRHEA-CNRS and Université Pierre et Marie Curie supported by the European Marie-Curie ITN Project CLERMONT4. Then he worked as a research associate at the University of Sheffield in the United Kingdom from 2014 to 2017 and joined Xi'an Jiaotong University in China as a professor in June 2017. His research interest focuses on light–matter interactions in microcavities and nanostructures.

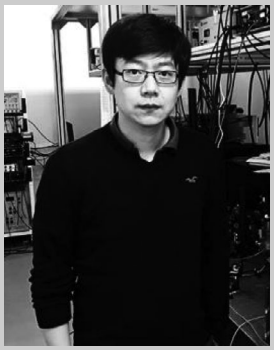

Yin Cai received the bachelor and master degrees in physics and optics from East China Normal University in China in 2008 and 2011, and a Ph.D. in physics from Ecole Normale Superieur Paris in France in 2016 with a joint Ph.D. from East China Normal University in 2017. Then he worked as a research associate at Nanjing University, China from 2017 to 2018, and joined Xi'an Jiaotong University in China as an associate professor in May 2018. His research interest focuses on light–matter nonlinear interactions in quantum optics.

Yanpeng Zhang received the Ph.D. in 2000 from Xi'an Jiaotong University, China. From 2001 to 2004, he was a postdoctoral fellow of the University of Connecticut, USA. Then he worked as a research associate at University of Arkansas, USA, from 2005 to 2007. Up to now, he is the professor and the leader of the Institute of Physical and Optoelectronics Technology, Xi'an Jiaotong University. His research interest focuses on the antibunching properties of atomic-like media and single quantum dots.

2. The Basic Theory, Design, and Construction of Open-Access Microcavities

2.1. Theory of the Mode Profiles

The concave-planar FP cavity supports Gaussian modes, which are characterized by the longitudinal and transverse profiles.

2.1.1. Gaussian Modes

We start from the wave nature of light. Assuming a small divergence angle of the optical beam, the electric field can be approximately described by the paraxial wave equation[19]

$$\nabla_{\perp}^{2} E(\boldsymbol{r}) + 2ik\frac{\partial E(\boldsymbol{r})}{\partial z} = 0 \tag{1}$$

in which $\nabla_{\perp}^{2}$ is the transverse Laplacian, $E(r)$ the electric field spatial distribution, and k the wavevector. $\boldsymbol{r} = \sqrt{x^2 + y^2 + z^2}$ defines the spatial coordinates and z is the beam propagation axis. The solution of the paraxial wave equation is given by

$$E(\boldsymbol{r}) = E_0 \frac{\omega_0}{\omega(z)} e^{-\frac{\left(x^2+y^2\right)}{\omega^2(z)}} e^{-ikz-ik\frac{\left(x^2+y^2\right)}{2R(z)}+i\phi(z)} \tag{2}$$

which is known as a Gaussian beam. ω_0 is the beam waist defined by the radius of the beam, or beam width, at its narrowest position of $z = 0$. $\phi(z)$ is the Gouy phase that quantifies the difference between the phase velocity of the Gaussian beam and the planar beam, $\omega(z)$ is the beam width and $R(z)$ is the radius of curvature (RoC) of the beam phase front that goes to infinity at $z = 0$.

Equation (2) describes a propagating Gaussian beam without any optical confinement. Inside the open-access microcavity, the geometrical configuration of the concave-planar mirrors determines a unique set of Gaussian modes, whose R(z) must match the RoC of the mirrors.

In this sense, the planar mirror specifies the position of the beam waist and the concave mirror set the boundary condition that determines the rest of the parameters of the Gaussian modes. To quantitatively link the Gaussian mode properties with the cavity geometry, the g parameter for each mirror is defined as

$$g_i = 1 - \frac{L}{R_i} \tag{3}$$

where L is the cavity length and R_i is the RoC of the mirrors with $i = 1, 2$ labeling the concave and planar mirrors, respectively. The beam waist is expressed by

$$\omega_0 = \left(\frac{\lambda L}{\pi}\right)^{\frac{1}{2}} \left(\frac{g_i g_2 (1 - g_1 g_2)}{(g_1 + g_2 - 2g_1 g_2)^2}\right)^{\frac{1}{4}} \tag{4}$$

which requires $0 \leq g_1 g_2 \leq 1$ known as the cavity stable criteria. As for the planar mirror $g_2 = 1$, Equation (4) reduces to

$$\omega_0 = \left(\frac{\lambda L}{\pi}\right)^{\frac{1}{2}} \left(\frac{R_1}{L} - 1\right)^{\frac{1}{4}} \tag{5}$$

and the beam waist locates on the surface of planar mirror. Equation (5) conveys two important principles for the design of open-access microcavities:

1) To confine light, the RoC of concave mirror must be larger than the cavity length, that is, $L < R_1$. This is the cavity stable criteria for concave-planar cavities.
2) The lateral mode size at a given cavity length, which is featured by the value of ω_0, decreases with R_1.

Additionally, in order to hold the Gaussian modes resonating inside the cavity, we need:

3) The physical size of the mirror has to be substantially larger than the mode size ω_0 to avoid high optical loss.

These three principles require that the mirror RoC, mirror size, and cavity length be considered together for cavity design. For example, while reducing R_1 to minimize ω_0, one has to reduce the cavity length at a certain point to satisfy the cavity stable criteria. Meanwhile, since the surface of the concave mirror is hemispherical, its size adds to the cavity length. It is both technically challenging to achieve very small mirror RoC during mirror fabrication and very small cavity length in the cavity structural setup (details in Sections 2.2 and 2.3), especially when the mirrors are made of DBRs, in which situation the cavity length has to be replaced by an effective length $L_{\text{eff}} = L + L_{\text{DBR1}} + L_{\text{DBR2}}$, where $L_{\text{DBR1,2}}$ are the penetration depth of the optical field into the DBR structures of the concave and the planar mirrors. In the reported experiments of light–matter coupling, the RoC of the concave mirror was usually chosen to be in a range between 5 and 70 μm to compromise between the targeted lateral confinement and technical capabilities.

The frequencies of the eigenmodes are expressed by

$$v_q = \frac{c}{2L}\left(q + \frac{1}{\pi}\cos^{-1}\sqrt{g_1 g_2}\right) \tag{6}$$

where the integer q is the cavity longitudinal order.

2.1.2. Transverse Profiles

Equation (2) presents a typical solution of the paraxial wave equation. In fact, the solution of the paraxial wave equation has several more general forms depending on the symmetry of the studied system in the x–y plane, referred as the transverse, or high-order, Gaussian modes. In the Cartesian coordinate, the solution is given by Hermite polynomials H_{nm}.[19]

$$E_{m,n}(x, y, z) = E_0 \frac{\omega_0}{\omega(z)} H_m\left[\frac{\sqrt{2}x}{\omega(z)}\right] \times H_n\left[\frac{\sqrt{2}y}{\omega(z)}\right] e^{\frac{\left(x^2+y^2\right)}{\omega^2(z)}} e^{-ikz-ik\frac{\left(x^2+y^2\right)}{2R(z)}+i(m+n+1)\phi(z)} \tag{7}$$

where m and n are integers indicating the Hermite polynomial order. Optical beams described by Equation (7) are referred to as Hermite–Gaussian (HG) beams. The HG beam exhibits a transverse field distribution characterized by Hermite polynomials, forming spatial patterns as shown in **Figure 2**a. The Gouy phase, given by $(m + n + 1)\phi(z)$ for HG mode, results in a series of transverse optical modes in the cavity eigenfrequencies.

$$v_q = \frac{c}{2L}\left(q + \frac{1}{\pi}(m + n + 1)\cos^{-1}\sqrt{g_1 g_2}\right) \tag{8}$$

Here (m, n) are named the transverse mode orders, indicating that HG modes specified by the same value of $(m + n)$ are degenerate. For the fundamental mode specified by $m = n = 0$, Equations (7) and (8) reduce to Equations (2) and (6), describing a Gaussian distribution of optical field in the transverse plane.

If we solve the paraxial wave equation in cylindrical coordinates with the transform $r = \sqrt{x^2 + y^2}$, $r(\cos\varphi \quad \sin\varphi) = (x \quad y)$,

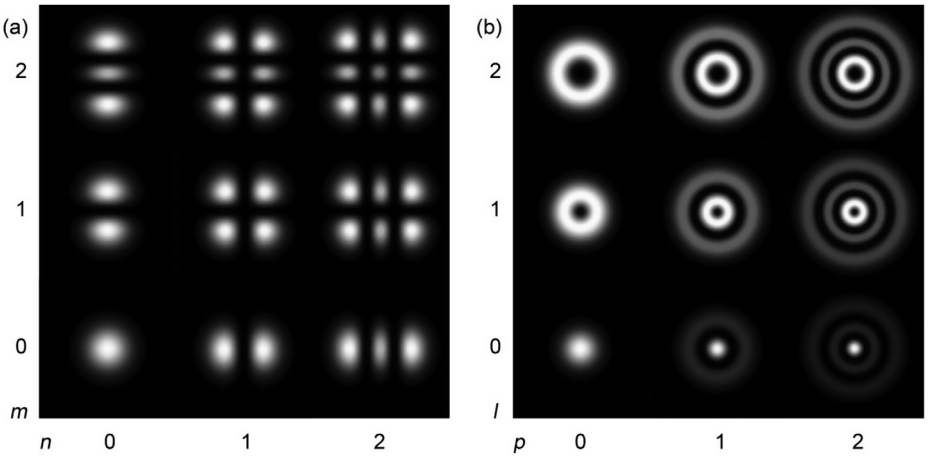

Figure 2. Lowest orders of a) Hermite–Gaussian (HG) and b) Laguerre–Gaussian (LG) modes.

the solution is expressed by associated Laguerre polynomials $L_p^{(l)}$.

$$E_{m,n}(r,\varphi,z) = E_0 \frac{\omega_0}{\omega(z)} \left(\frac{\sqrt{2}r}{\omega(z)}\right)^{|l|} \times L_p^{(l)}\left[\frac{2r^2}{\omega^2(z)}\right] e^{il\varphi} e^{\frac{-r^2}{\omega^2(z)}} e^{-ikz-ik\frac{r^2}{2R(z)}+i(2p+|l|+1)\phi(z)} \quad (9)$$

where p and l are integers indicating the orders of the Laguerre polynomials. Optical beams described by Equation (9) are referred to as Laguerre–Gaussian (LG) beams. The dependence of the optical phase on φ reveals that the LG beams with nonzero l carry orbital angular momentum (OAM). The Gouy phase $(2p + |l| + 1)\phi(z)$ indicates that LG mode specified by the same value of $(2p + |l|)$ are degenerate. At $p = l = 0$, Equation (9) reduces to Equation (2) describing the fundamental Gaussian mode. The spatial profile of several lowest orders of LG modes are shown in Figure 2b.

The actual mode profiles of the open-access microcavities depend on the boundary conditions resulting from the cavity shape, that is, cavity mirrors exhibiting Cartesian (resp. circular) symmetry leads to HG (resp. LG) modes. As the concave mirrors of the open-access microcavities are designed with a circular shape, LG modes are expected. Nevertheless, as asymmetries are inevitably induced during the fabrication process, mirrors usually exhibit a slightly elliptical shape, which breaks the LG mode degeneracy and supports Mathieu–Gaussian (MG) or Ince–Gaussian (IG) modes,[20] whose spatial distributions are similar to HG modes at small transverse orders but with lifted degeneracy in eigenenergies.

2.1.3. Quantum Description of the Cavity Embedded with Excitons

One of the elementary excitations in semiconductors is the exciton, a bound state of an electron and a hole via Coulomb interaction that can be created and annihilated by absorbing and emitting a photon. The cavity with an exciton inside is described by the Hamiltonian of the coupled system[21]

$$H = \hbar\omega_c \hat{a}^\dagger \hat{a} + \hbar\omega_X \hat{b}^\dagger \hat{b} + \hbar g\left(\hat{a}^\dagger \hat{b} + \hat{b}^\dagger \hat{a}\right) + \hbar\alpha \hat{b}^\dagger \hat{b}^\dagger \hat{b}\hat{b} \quad (10)$$

where $\hat{a}$ and $\hat{b}$ are the annihilation operators of a cavity photon and an exciton respectively, and ω_c and ω_X are the resonance frequencies of the cavity and exciton modes. The third term describes the exciton–cavity coupling, which adds off-diagonal elements to the Hamiltonian, resulting in new eigenstates for the coupled system named exciton-polaritons. g is referred to as the photon–exciton coupling strength, determined by the exciton oscillator strength and the spatial overlap between the exciton and photon wavefuctions.[22] The last term describes the Kerr-type nonlinearity arising from Coulomb interaction between excitons and from Pauli exclusion effects,[21] which is a key factor leading to nonlinear and quantum effects of exciton-polaritons.

In the open-access microcavity that supports a series of transverse Gaussian modes with different ω_c, each cavity mode only strongly couples with the exciton mode that have the same spatial wavefunction and wavevector distribution.[21,23] Therefore, Equation (10) applies to each transverse cavity mode individually. The main consequence of the multiple cavity mode system is that different modes of exciton-polaritons coexist at different energy levels.

2.2. Cavity Mirror Fabrication

Whilst the DBR coating that ensures high reflectivity of the cavity mirrors follows standard material growth or deposition technologies, the most special and significant fabrication technique developed for the open-access microcavities is the fabrication of micro-sized concave mirrors, which generally exhibit hemispherical surfaces with RoC fitting the phase front of confined Gaussian modes at the beam center. Laser ablation and focused ion beam (FIB) milling are the two most widely adopted methods that we will mainly focus on in this review.

2.2.1. Early-Stage Fabrication Methods

The early-stage fabrication methods mainly include wet-etching, lift-off coating, and latex sphere–assisted deposition, which initiate the studies of open-access microcavities and encouraged the development of more sophisticated fabrication methods.

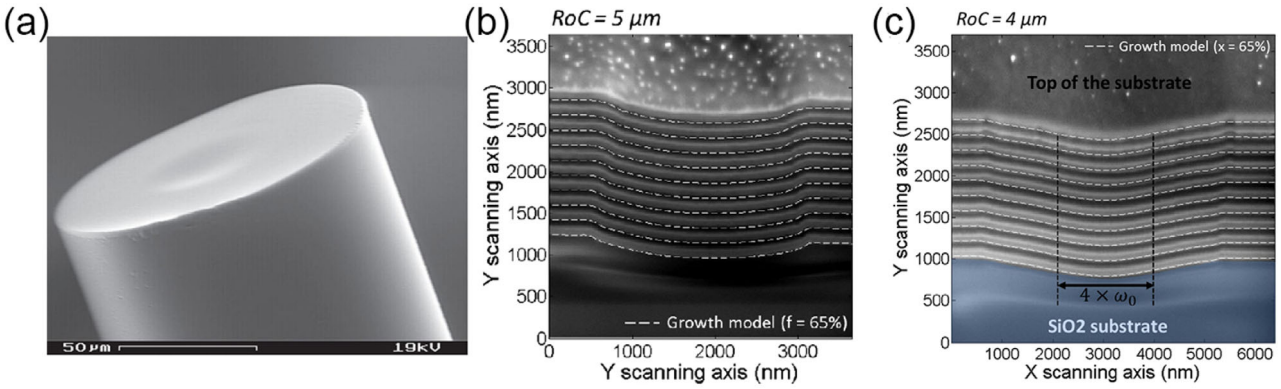

Figure 3. Scanning electron microscopy (SEM) images of concave mirrors. a) Concave mirror fabricated by laser ablation on an optical fiber facet. Reproduced with permission.[40] Copyright 2010, IOP Publishing. Cross-sections of the b) hemispherical and c) Gaussian isophase concave mirrors fabricated by FIB milling on silica substrate, deposited with dielectric DBRs. The dashed white lines show the simulated results of the DBR growth model. The particles on the concave surface results from a metal coating for clear SEM imaging and are absent for the application of the concave mirrors. Reproduced with permission.[32] Copyright 2015, OSA Publishing.

Wet Etching: The earliest open-access microcavities, designed for atomic physics, is reported by Trupke et al. in 2005,[24] in which the microscale concave mirror is fabricated by wet etching. An approximately spherical surface profile is produced using a mixture of HF and HNO_3 in acetic acid through circular apertures in a lithographic mask.

Lift-Off Coating: In 2006, Steinmetz et al. reported a novel method for fabricating microscale concave mirrors using lift-off coating.[25] In this process, a convex surface of silicon microlens is deposited with a stack of dielectric DBR, then the center of the microlens is positioned to the facet of a cleaved optical fiber and glued in place with an UV-curing epoxy. The DBR mirror is then detached from the original substrate with a small force, leaving a concave-surfaced DBR mirror at the fiber facet. It is worth to mention that it is the authors of this work who developed the laser ablation method years later, in both fiber-based and chip-based microcavity systems.

Latex Sphere–Assisted Deposition: The pioneer work by Pennington et al. reported a fabrication method for metal-coated concave mirrors by structuring a template of latex spheres on thin film of gold.[26] After the spheres adhere to the substrate surface, another layer of gold thin film is grown around them, leaving spherical "dishes" when the spheres are washed away. LG modes were observed from the resulting open-access microcavity.

All the above methods developed in the early stage of open-access cavity systems enable easy and fast fabrication, but do not allow precise control of the concave shape and bring difficulties in fabricating mirrors with small RoC. Therefore, they were later replaced by the more advanced methods of laser ablation and FIB milling.

2.2.2. Laser Ablation

The fabrication process using CO_2 laser ablation on optical fiber facets was introduced by Hunger et al. initially in atomic Bose–Einstein condensation (BEC) experiments, and is widely adopted for open-access microcavities. The basic principle is that the intensity profile of a focused laser beam can be transferred onto a silica substrate or an optical fiber facet via surface melting and resolidification.[27] A good combination of the laser power and exposure time is the key factor to obtain smooth surface and desired shape of the concave surface. In short laser pulse with high power, the ablated area is resolidified faster than the thermal smoothing process, resulting in increased surface roughness. In the opposite case, the melted area extends deeply into the material resulting in undesired morphological features.[28] The resulted dimple exhibits a Gaussian profile in depth, which can be approximated by a hemisphere with a uniform RoC at the center region, as shown in **Figure 3**a. The concave surfaces fabricated by laser ablation in the reported literatures demonstrates RoC ranging from 7 to 200 µm and diameters ranging from 8 to 60 µm, with the lowest root-mean-square (RMS) surface roughness of 0.18 nm.[28] The laser ablation method is fast and produces smooth surface, however, its resolution is limited by the laser beam, which makes it challenging to fabricate high-quality mirrors with small RoC.

Very recently, an alternative fabrication method was reported by first creating a rough concave shape with wet etching on an optical fiber facet, followed by selective heating and reflow with CO_2 laser ablation to smooth the surface. Such fabrication method leads to a small RoC of 4.7 µm with smooth surface (RMS roughness ≈0.1 nm).[29]

2.2.3. Focused Ion Beam Milling

FIB milling was developed as a more precise method for fabricating microscale concave mirrors by Dolan et al. in 2010,[30] around the same time as laser ablation was applied. In an FIB, Ga ion beam is used to etch materials under high resolution with a beam size, which increases with applied beam current, of 5–100 nm. At a given beam current, the dwell time determines the etched depth. By varying the dwell time of the FIB etching as a function of position, the Ga ion beam creates a concave surface.[31] In the experiment, the field of view is digitized into a matrix of pixels, within which a pattern of 2D array of concave mirrors can be fabricated. A greyscale colormap quantifying the dwell time at each

pixel is loaded into the control system of the FIB to program the pattern. Both the magnification of the colormap and the applied current beam has to be carefully chosen to fit the desired structure; while increasing the magnification and the current beam shortened the processing time, it reduces the resolution of the fabrication.[31]

Topographic Control: The main advantage of FIB milling is the high resolution that allows free control of the details of the fabricated structures. Trichet et al. highlighted this by demonstrating the topographic control of the concave mirrors for open-access microcavities.[32] While being able to fabricate hemispherical mirrors, they show the ability of sculpturing the concave shape with high resolution to fit exactly a targeted phase front of a Gaussian beam. The SEM images of hemispherical and Gaussian isophase (GI) concave mirrors are shown in Figure 3b,c, showing clear topographical differences. The design of GI surfaces is crucial for small concave mirrors with RoC <7 μm as deviation of hemispherical surfaces from the phase front becomes significant. For open-access microcavity with GI concave mirrors, the targeted length[32] is an important parameter for the design of the targeted GI surface, which defines the optimum cavity length the open-access microcavity should work with.

The FIB milling allows to reach a concave surface with a physical RoC as small as 1 μm, and the surface roughness can reach smaller than 0.7 μm of RMS.[31] The precise control and high resolution being its advantages, it takes long processing time and may introduce impurities by the Ga ions.

2.2.4. Planar Mirrors

The fabrication of the planar mirror depends on the nature of the in-cavity emitter. For an emitter that can be directly grown on DBRs, such as InGaAs quantum dots (QDs) and quantum wells (QWs), a GaAs/AlGaAs semiconductor DBR can be grown by molecular beam epitaxy. On the other hand, for materials that are not integrated to any monolithic DBR, such as TMD monolayers and color centers in diamond, the best way is to first deposit a dielectric DBR, for example, consisting of SiO_2/TaO_5, on a silica substrate by standard deposition method such as e-beam (electron beam) evaporation and DC (direct current) sputtering, and then transfer the active material onto the DBR by spin-coating or exfoliation. The concave mirror does not hold active materials and is therefore deposited with dielectric DBRs.

It shall be noticed that the open-access microcavities can also have both mirrors planar which support 2D polaritons, without needing the fabrication of concave mirror. If the mirror surface contains both planar and concave features, 0D and 2D polaritons coexist. Trichet et al. demonstrated the coupling between the confined 0D mode and 2D optical modes at large longitudinal orders.[33]

2.3. Cavity Structure

Two types of cavity structures are widely used, specified by the supporting material of the concave mirrors. The mirrors can be fabricated on a cleaved facet of an optical fiber and on a solid substrate, referred to as fiber-based and chip-based open-access microcavities in this review, each showing its own advantages and suitable applications. For each structure type, the setup can be designed either for reflectivity configuration, that is, excitation and collection from the same side of the cavity or transmission configuration, that is, excitation and collection from different sides.

2.3.1. Fiber-Based Cavity Structure

Fiber-based open-access microcavities, also referred to as fiber cavities,[34] were firstly invented for holding small-volume standing optical waves in atomic systems in 2005,[24,25] which allows to achieve strong atomic field coupling of BEC in 2007.[35] In these works, the concave mirrors were fabricated by wet etching or lift-off coating. These early-stage developments of the fiber cavity systems, through the collaboration between several European labs, are of great historical importance of being transferred to a wide range of applications in solid-state optical systems. In 2009, Muller et al. from the University of Maryland introduced the fiber cavity fabricated by lift-off coating to host solid-state quantum emitters, that is, InAs QD,[36] and developed an ultra-high-fineness double-concave fiber cavity based on laser ablation in 2010.[37] The fiber cavity by laser ablation was started to be applied for exciton-polaritons by Besga et al. at ETH Zurich in 2015.[34]

Figure 1a sketches the fiber-based cavity structure. In the setup the fiber is fixed and a 3D stack of nanopositioners are used to control the *xyz* position of the planar DBR to form a concave-planar cavity. In the reflectivity configuration, both the excitation beam and the collected light go through the fiber, as the cavity mode directly couples to the fiber core where the concave mirror is located. Alternatively, the fiber cavity can work in the transmission configuration by placing a lens with motion control at the planar DBR side to collect the transmitted light.

2.3.2. Chip-Based Cavity Structure

In 2010, Dolan et al. at the University of Oxford reported the first chip-based open-access microcavity which contains concave mirror arrays fabricated by FIB milling on a silica substrate.[30] Meanwhile, in 2011, Barbour et al. at the University of Basel adopted the laser ablation method, previously applied in fabricating fiber cavities, to fabricate a tunable cavity with a concave mirror of RoC = ≈100 μm on a silica substrate,[27] which is further improved to enable small RoC and enhanced mode matching in 2014.[38] The chip-based cavities enable full free-space excitation and collection, followed by numerous research groups for holding various light-emitting materials. Almost simultaneously as the fiber cavity, the chip-based cavity starts to be applied for exciton-polaritons by Dufferwiel et al. at the University of Sheffield in 2014.[39]

Figure 1c sketches the chip-based cavity structure. It is not enough to reach a sufficiently short cavity length just by contacting the two substrates that contain the planar and concave mirrors, as the slight nonparallelism of the two substrates may result in a big gap between the mirrors when the edges of the substrates touch first, considering the macroscale size of the substrates. Therefore, reducing the contacting area of the substrates becomes significant. To address this issue, a sub-millimeter-sized

plinth, for example, 0.3 mm in length, width, and height, is made by mechanical dicing or carving on the host substrate such as silica. Then arrays of concave mirrors are fabricated on the surface of the plinth, as illustrated in Figure 1c. The chip-based structure enables full free-space optical measurements. In the reflectivity configuration, a fixed lens is used for both excitation and collection, while the concave and planar mirrors are controlled by two independent stacks of nanopositioners, allowing both cavity tuning and focus adjusting. To achieve the possible minimum cavity length, two goniometer nanopositioners are added into the control stack of the planar mirror, in addition to the *xyz* control.[39] This allows fine tuning of the relative tilt angle between the concave and planar mirrors to reach perfect parallelism, which is crucial for achieving short cavity length. The setup becomes more complicated for transmission setup, as a collection lens needs to be added with independent motion control.

2.3.3. Comparison between the Two Types of Structures

It is useful to be aware of the advantages and disadvantages of the fiber- and chip-based structures to ensure the optimal choice for the studied physical system.

The assembling setup of fiber-based cavity is much simpler: it requires one less nanopositioner stack than the chip-based cavity, which helps to reduce mechanical noise. Meanwhile, due to the flexibility of the optical fiber, the fiber cavity is more convenient to switch between the reflectivity and the transmission configurations, especially for low temperature operation that relies on space-limited vacuum systems. The relatively easy realization of transmission configuration renders the fiber cavity a straightforward choice for resonant excitation at low temperature.

Nevertheless, the chip-based cavities have a few advantages. Compared to fiber excitation, free-space optics allows high pumping power and less dispersed ultrafast pulses, which works better for studying nonlinear effects and ultrafast dynamics. Compared to fiber collection, free-space optics is more convenient for space, polarization, and time-resolved imaging. The chip-based cavities also allow design of spatial patterns such as coupled cavity arrays, not limited by the size of the fiber core.

Another interesting issue is the photon collecting efficiency, which is significant for quantum emitters. In the fiber-based cavities, the fiber core directly connects the cavity photons, polarization control, and detectors, avoiding losses from substrate surface reflections and free-space optical elements expected in the chip-based cavities. However, it is shown that at small RoC (<10 μm) of the concave mirror, the spatial mismatching between the fiber-guided mode and the cavity Gaussian mode becomes dominant,[40] leading to a critical drop of the collection efficiency, which is nevertheless not a problem for free-space optics with a decent collection numerical aperture. **Table 1** gives a summary of the cavity fabrication methods and structure types from some of the research groups that performed investigations with open-access microcavities.

2.3.4. Cryogenic Setups

In most cases, the active materials need to work at low temperature to serve as quantum emitters or create exciton-polaritons, in which situations cryogenic setups are required. This can be done by loading the open-access microcavity setup in a metal vacuum tube filled with low-pressure helium (He) gas, with controlling electronic wires and optical fibers connected out through vacuum-sealed ports. The vacuum tube is then inserted into a liquid He dewar, forming a bath cryostat that cools the whole system to ≈5K (**Figure 4**a,b).[41] For k-space imaging, extra lenses are loaded inside the vacuum tube to make a fully confocal optical system, as sketched in Figure 4b.[39] For the chip-based cavities, the transmission setup working at 5 K can be established by aligning cavity mirrors vertically in He gas-filled vacuum chamber which is cooled via a metal plate contacting liquid He, as sketched in Figure 4c.[42]

Table 1. Summary of the cavity fabrication methods and structure types of open-access microcavities adopted in various research groups.

Structure\concave mirror	Laser ablation	FIB milling
Fiber based	1, 2, 6, 7, 12	8
Chip based	3, 11	4, 5, 8, 9, 10, 13

Affiliations: 1) Laboratoire Kastler Brossel; 2) University of Maryland; 3) University of Basel; 4) University of Oxford; 5) University of Sheffield; 6) ETH Zurich; 7) Ludwig-Maximilians-Universität; 8) Max Planck Institute for the Science of Light; 9) IBM Research—Zurich; 10) University of Würzburg; 11) University of South Florida; 12) Macquarie University; 13) Imperial College London.

2.3.5. Mechanical Stability

The cavity stability issue arises from the relative vibrational motion between the two cavity mirrors, which results in fluctuation of the cavity length, and thereby linewidth broadening and peak intensity quenching of cavity modes. The mechanical noise can come from the floor vibration, environmental acoustic noise, He boiling inside the cryogenic dewar, the vibration of optical tables and nanopositioner stacks, etc.[39] The noise spectra were measured by Dufferwiel and Fink for the chip-based and fiber-based open-access microcavities indicates mainly low-frequency vibrations below 250 Hz.[28,39]

It is worthwhile to mention that the linewidth broadening induced by mechanical vibrations is not related to any intrinsic property of the studied physics, as the lifetimes of cavity photons and emitters, usually in pico to nanoseconds, are much shorter than the vibrating cycle. Nevertheless, most of the measurements for quantum emitters and polaritons require long integration time to reach an acceptable signal to noise ratio, and cavity stabilization is required if the cavity is designed for a *Q*-factor sufficiently high that could be seriously influenced by the vibration.[43] One of the most commonly used method of passive stabilization is touching the concave and planar mirrors, which greatly reduces their relative motion.[39] Despite the stability issue, open-access microcavities show comparable *Q*-factor with monolithic microcavities, ranging typically between 20 000 and 50 000 depending on the details of the cavity mirrors such as the number of DBR bilayers and DBR materials.

Active stabilization of the cavity length was also developed more recently. Trichet et al. used the laser transmission at the edge of the DBR stopband to monitor and control the cavity

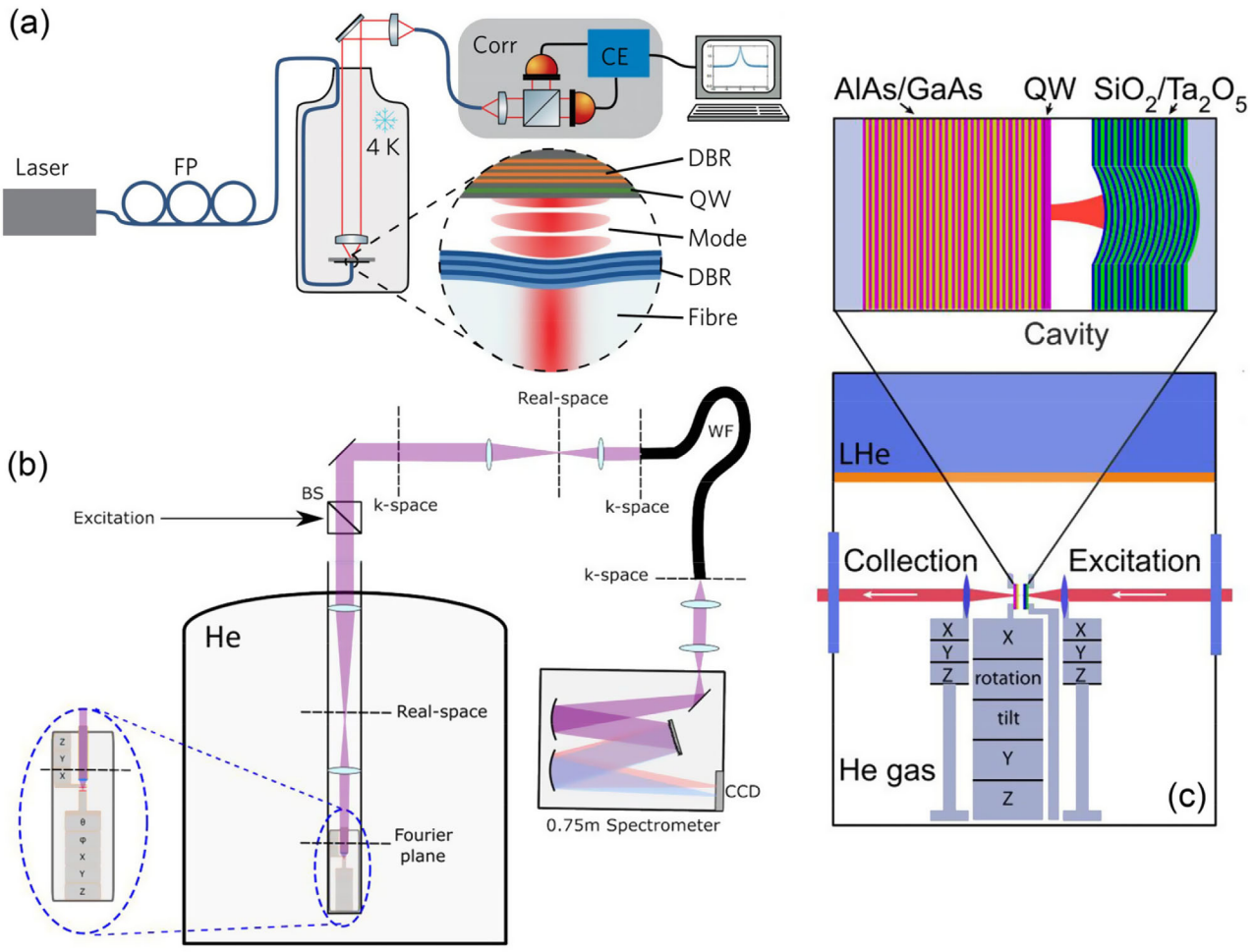

Figure 4. Cryogenic setups for open-access microcavities. a) Fiber-based open-access microcavity in transmission configuration. Reproduced with permission.[41] Copyright 2018, Springer Nature. b) Chip-based open-access microcavity in reflectivity configuration. The setup has all lenses confocal and can be used for both real space and k-space imaging. Note that there is a short-focus lens located closely above the sample (blue colored in the inset) for light collection, at the back focal plane of which the Fourier image of k-space is located. Reproduced with permission.[89] Copyright 2015, APS. c) Chip-based open-access microcavity in transmission configuration. Reproduced with permission.[42] Copyright 2018, AIP Publishing.

length in real time with a 50 Hz feedback loop on a DC piezoelectric stack.[44] Wang et al. introduced a feedback mechanism based on the Hänsch–Couillaud technique using a "locking laser," which reduced the RMS vibration amplitude from 2 to 0.1 nm, enabling the achievement of a very high Q-factor of 230 000.[45]

2.4. Cavity Shape Design and Spectral Engineering

In addition to hemispherical shape, the concave mirror can be designed with various shapes that allow to engineer the optical spectrum and loss. A number of works have reported spectral splitting of transverse Gaussian modes due to the slight ellipticity of the concave mirror induced in the fabrication processes.[34,46,47] Benedikter et al. studied specifically the mode profiles in a fiber-based cavity with a concave mirror of an elliptical shape, a typical result of laser ablation fabrication, showing large RoCs of 161 and 201 µm in the long and short axes.[48] The authors found that the nonideal mirror shape and finite size leads to linewidth broadening, eigenenergy shifts, and shape distortions of the cavity modes, especially at large cavity lengths where the fundamental Gaussian mode is coupled with the more lossy transverse modes of a higher longitudinal order. These studies revealed the possibility to use engineered concave mirror shapes to control the in-cavity light–matter interaction.

Flatten et al. carried out a thorough study on the influence of concave mirror shapes on cavity mode profiles and eigenenergies in 2016.[49] In this study, chip-based concave mirrors of hemispherical shapes were fabricated with a small RoC = 6 µm. With the high precision of fabrication enabled by the FIB milling, the authors geometrically brought a pair of hemispherical mirrors to partially overlap that form coupled open-access microcavities, which was also studied for exciton-polariton systems by Dufferwiel et al. in 2015.[50] By varying the center-to-center distance between the two mirrors, the entire shape changes in the sequence (**Figure 5**a): 1) two single hemispheres; 2) coupled hemispheres; 3) elliptical concave shape; and 4) a single hemisphere. A complete tracing of the mode profiles and eigenenergy splittings

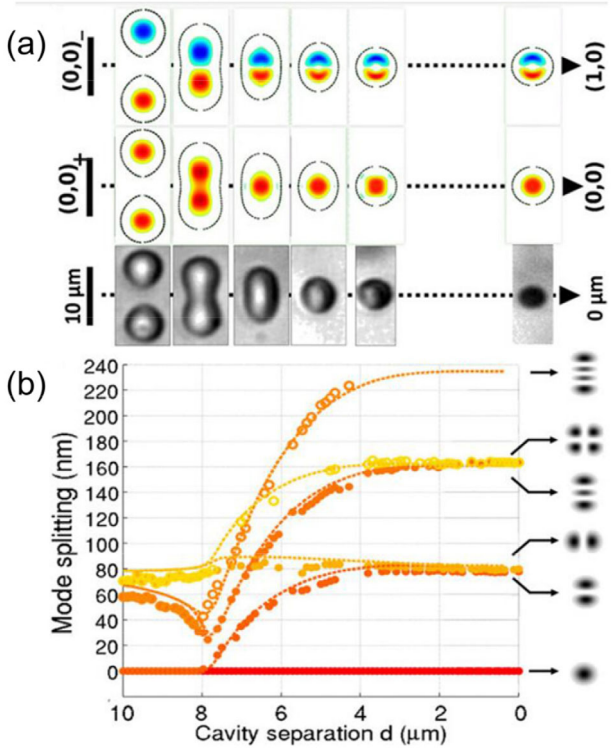

Figure 5. Spectral engineering of open-access microcavities by bringing two circular-shaped concave mirror into overlap. a) Field distribution of the hybridization of the first bonding and antibonding cavity modes (upper two rows) and microscope images (lower row) while varying the distance between two circular-shaped concave mirrors. b) The mode profiles and eigenenergy splittings throughout this change, the dot and dashed lines representing the experimental results by laser transmission and simulation by mode mixing formalism, respectively. Reproduced with permission.[49] Copyright 2015, Wiley-VCH.

throughout this change are presented, as shown in Figure 5b. The authors also trace the change of high-order transverse mode, among which the coupling effects are demonstrated. The experimental results can be well explained by the mode-mixing formalism developed by Kleckner et al.[51] The studies by Flatten et al. provides a systematic methodology of designing cavity structures to control the mode profiles and spectral properties, ready to be applied in landscape tailoring for the light–matter interaction in open-access microcavities.

3. Exciton-Polaritons in Open-Access Microcavities

We will first review in general the studies of exciton-polaritons in microcavities in Section 3.1, and then focus on the specific achievements of exciton-polaritons in open-access microcavities, which cover Sections 3.2–3.4.

3.1. Exciton-Polaritons

A basic description of exciton–photon coupling has been introduced in Section 2.1.3. In reality, both the exciton and the cavity photon exhibit finite lifetimes subjecting to various decay mechanisms. A bright exciton can be either strongly or weakly coupled to a photon, depending on whether the coupling strength g exceeds their decay rates. In the weak coupling regime, the light–matter coupling can be treated as a perturbation that modifies the lifetimes of the exciton and the photon, leading to enhanced or suppressed spontaneous emission known as the Purcell effect.[4] In the strong coupling regime, new eigenstates named exciton-polaritons form, characterized by a vacuum Rabi splitting in eigenenergies, as illustrated in **Figure 6**a. The exciton-polariton is a coherent superposition of the bare exciton and photon states, exhibiting a mixed nature of light and matter. By varying the detuning between the photon and exciton energies, one can successively tune the physical property of exciton-polaritons from more excitonic-like to photonic-like, determined by the corresponding Hopfield coefficients illustrated by Figure 6b.

The microcavity is among the most advantageous systems for investigating exciton-polaritons due to its long photon lifetime and small mode volume that allows maximizing the spatial overlap between the exciton and photon wavefunctions.[52] Since the first observation of cavity polaritons by Weisbuch et al. in 1992,[53] numerous exciting advances has been demonstrated in the past few decades. The BEC of cavity polaritons as Bosonic particles was demonstrated in 2006,[54,55] followed by the observation of quantized vortices[56–58] and superfluidity[59,60] in the polariton condensate. The nonlinearity of polaritons, that is, particle–particle interaction inherited from the excitonic component (described by the last term of Equation 10)), becomes the focus of interest on polariton research. In addition to the fact that the polariton nonlinearity enables dark[61] and bright solitons[62] as some other nonlinear optical systems do, one can simply use the pump light or the designed cavity nanostructures to tailor excitonic and photonic potential landscapes that enables on-chip manipulations of light.[63–65] Moreover, the transverse electric–transverse magnetic (TE–TM) mode splitting and external magnetic field are demonstrated to affect the polaritonic spin via the photonic and excitonic parts respectively,[9,66,67] which eventually led to the demonstration of polaritonic topological insulators.[8,9,68,69]

3.1.1. Quantum Effects of Exciton-Polaritons

All the achievements discussed above render cavity polaritons a promising system as quantum simulators for complex physical systems. Meanwhile, the strong nonlinear effects of cavity polaritons also make it a good candidate for on-chip quantum information. In order to initialize the polariton system in a known quantum state, one needs to demonstrate nonclassical polaritons as the first step. With such consideration, efforts have been made for realizing both squeezed polaritons in the continuous variable regime and single polaritons.

Quantum Squeezing and Fluctuation: The idea of quantum effects of polariton was proposed and thoroughly investigated by Eleuch et al. in 1999, in which quantum effects such as squeezing and photon antibunching are predicted for resonantly pumped cavity polaritons due to the excitonic nonlinearity.[21] The authors further pointed out that the quantum effects could be destroyed by strong exciton-phonon scattering. Indeed, squeezed polariton states were demonstrated experimentally via a four-wave-mixing

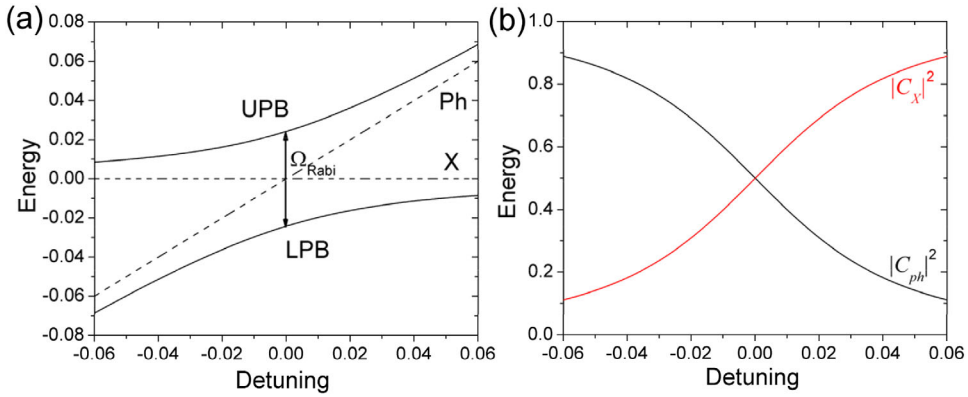

Figure 6. Formation of exciton-polaritons. a) Anticrossing featured by the vacuum Rabi splitting (Ω_{Rabi}) results from the strong coupling between the cavity photon (Ph) and exciton (X), leading to new eigenstates of the upper polariton branch (UPB) and the lower polariton branch (LBP). The graph uses normalized energy units with respect to the exciton energy, that is, $E_{norm} = (E - E_X)/E_X$. b) The Hopfield coefficients of the LPB, characterizing the excitonic ($|C_X|^2$) and photonic ($|C_{ph}|^2$) fractions of the exciton-polariton, are plotted as a function of the detuning between the photon and exciton energies.

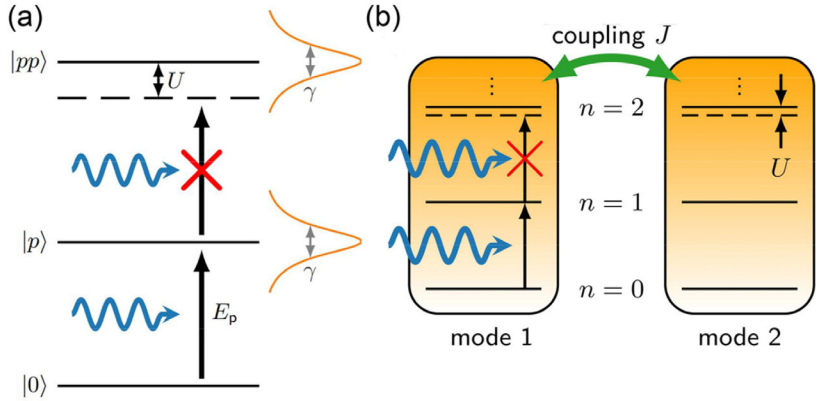

Figure 7. Schematics of polariton quantum blockades. a) Conventional blockade in which the nonlinear interaction between two polaritons blocks the excitation of a second polariton when $U > \gamma$. Reproduced with permission.[28] Copyright 2018, ETH Zurich. b) Unconventional polariton blockade in which the coupling J between two cavities reduces the required polariton nonlinearity U. Reproduced with permission.[93] Copyright 2011, APS.

process at the optical bistability regime, reported with 6% intensity squeezing by Karr et al. in 2004[70] and 20.3% intensity squeezing by Boulier et al. in 2014.[71] In 2018, Jabri et al. proposed a novel method to enhance the polariton squeezing using a coupled double QW strongly coupled to cavity photons.[72] The authors showed that the nonlinear interactions in the direct and indirect excitonic modes could lead to significant squeezing despite weak nonlinearities, and the dominant contribution to the noise spectra of the system came from the indirect excitons in the strong exciton–photon coupling regime.[72]

Quantum Blockade Effect: Another significant step on the way to quantum polaritonics is the demonstration of single particle state and single particle interaction in polariton systems, for which the idea of polariton blockade is proposed.[73] As illustrated in **Figure 7**a, the nonlinear interaction between two polaritons leads to an energy blueshift of the two-excitation manifold, which blocks the possibility of simultaneously injecting more than a single polariton. This scenario, nevertheless, can only occur in the situation where the interaction energy of two polaritons U exceeds the polariton linewidth γ, which is extremely challenging due to technical limits.

Unique Merits of the Open-Access Microcavity System for Quantum Polaritonics: In the polariton squeezing measurement reported in ref. [71], 3D optical confinement, enabled by the micropillar structure, is well applied to enhance the polariton–polariton interaction, which prevents the motion driven by the repulsive potential and keeps a maximum overlap of polariton wavefuctions. On the other hand, while the microcavity is etched into micropillars for tight lateral confinement, the etching into the active media broadens the excitonic linewidth, resulting in a dilemma for the quantum blockade demonstration. It therefore requires a device that provides strong 3D light confinement while keeping the active media unaffected, for which the open-access microcavity appears as a perfect choice. First of all, the lateral confinement by the concave-planar cavity structure, which can reach a sub-micron lateral mode size, does not involve any etching on the active media. Moreover, the confinement potential can be much deeper than that provided by micropillars. Besides providing strong 3D confinement, these merits of open-access microcavities allow flexible structuring of polariton potential landscapes, enabling new methods for spatial and pseudospin control of polaritons. Moreover, the freedom of embedding

foreign emitters render it a versatile tool for polaritonics based on a large variety of materials that exhibit advantageous optical properties. Especially, the potential ability of embedding novel emitters of very strong nonlinearity inside high-quality microcavities would eventually lead to giant advances in quantum polaritonics.

3.1.2. Exciton-Polaritons as a Driven-Dissipative System

As quasi-particles, exciton-polaritons form a driven-dissipative system due to the finite lifetime inherited from the excitons and cavity photons, in which the creation and decay of a polariton is via the interaction of its external environment such as the exciton reservoir. The dissipative nature makes the polaritons differ from the ideal BEC system that is supposed to be in thermal equilibrium. For example, unlike the ideal BEC whose critical density is determined by the particle mass and temperature, the condensation of polaritons at a given temperature is determined by a mechanism of kinetics versus thermodynamics, leading to an optimal exciton–photon detuning at which the lowest condensation threshold is obtained.[74–76] In many of the investigations on the collective behaviors of exciton-polaritons, the system is often viewed approximately as a closed one, that is, the investigated physical process does not include the interaction of the system with its environment as a significant part. Nevertheless, such interaction can be very important and lead to new scenarios of physics. Eleuch and Rotter systematically studied the quantum resonances in open systems, of which the Hamilton operator becomes non-Hermitian due to the dissipative nature.[77] The quantum states of the open system may couple via the common environment, exhibiting complex eigenvalues and biorthogonal eigenfunctions. The most interesting property of the open system is the so-called exceptional point (EP) in the parameter space, a singularity at which the eigenvalues of two states coalesce, corresponding to the same eigenfunctions.[78,79] Around the EP, the non-Hermitian Hamiltonian can result in avoided level crossing of eigenvalues and bifurcation of widths (lifetimes), as well as a variation of the phase rigidity of the eigenfunctions. While the observation of EP and related physical processes have been reported in different systems including microwave cavities, open QDs, single-electron transistors, and atomic assembles,[80] its application in photonics has also been explored in recent years.[14,81] Particularly, the experimental investigation of the non-Hermitian nature and observation of EP in exciton-polaritons were reported by Gao et al. in 2015 in an optical-induced billiard potential designed on a monolithic microcavity.[82] It is thereby expected that the free design of photonic potentials with strong confinement enabled by the open-access microcavity would help to further explore the exciton-polaritons as a dissipative open system.

Another interesting investigation related to the driven-dissipative nature is the analysis of the photon transport through the microcavities. Wang and Taylor built the theoretical models to study the flow of photons in a photonic system coupled to two external reservoirs as well as with a center mesoscopic region, enabling a direct photonic analog to electron transport driven by a voltage bias in electronic devices.[83] Recently, Mantsevich and Glazov established theoretical models to describe the fluctuations of tunneling currents in photonic and polaritonic systems.[84] The authors obtained noise spectra for photon tunneling transport directly between two reservoirs, as well as passing through noninteracting and interacting intermediate regions between the reservoirs, in which the microcavity in the strong coupling regime was proposed as an suitable system for experimental realization. Indeed, Rodriguez et al. reported experimental demonstration of hopping phase in coupled photonic microcavities, by considering the driven-dissipative nature of the exciton-polaritons.[85] Experimental studies based on more sophisticated theoretical models would be expected with further progress in polariton landscape engineering.

3.2. Exciton-Polaritons in Epitaxial QWs in Open-Access Microcavities

Arsenide QWs are the most widely used optical media for the investigation of exciton-polariton physics, thanks to the direct homoepitaxial growth of QW layers on highly reflective AlGaAs/GaAs DBRs that enables long coherence lifetime of QW excitons at low temperature. The structural sketches in Figure 4 are also good illustration of the GaAs-based open-access microcavities. The semiconductor sample contains the planar AlGaAs/GaAs DBR on a GaAs substrate, on which InGaAs or GaAs QWs are grown at the optical field antinodes of the designed cavity.

3.2.1. Demonstration of Strong Coupling

The strong light–matter coupling of InGaAs QWs in the chip-based and fiber-based open-access microcavities were first demonstrated by Dufferwiel et al.[46] in 2014 and Besga et al.[34] in 2015. The signature behaviors of anticrossing between the QW exciton and the cavity photon were demonstrated by tuning the cavity length (example in **Figure 8**a), showing a maximum vacuum Rabi splitting of 5.6 meV (6 QWs) and 3.4 meV (single QW), respectively. In fact, the vacuum Rabi splitting is a tunable property in the open-access microcavities as the exciton–photon wavefunction overlap is directly related to the length of the air gap between the mirrors, given by $\Omega_{\mathrm{Rabi}} \propto 1/\sqrt{L + L_{\mathrm{DBR}} + L_{\mathrm{QW}}}$, where L, L_{DBR}, and L_{QW} are the lengths of the air gap, QW region, and DBR penetration. Good agreements were reported between the experimental and simulated values of Rabi splitting as a function of cavity length (Figure 8c).

The investigation of spatial mode profile was enabled by the chip-based cavity setup. LG type transverse modes were clearly observed when imaging the cavity modes with low spectral resolution (Figure 8b). Nevertheless, at high spectral resolution, the actual lift of degeneracy was revealed by spectral splittings into a family of Mathieu and Ince–Gaussian modes, due to the imperfection of the concave mirror shape that broke the circular symmetry.[46]

3.2.2. Spin Vortices

The open-access microcavity is a natural tool for investigating polaritonic vortices[56–58,86,87] due to the fact that higher-order LG modes carry nonzero OAMs. Especially, the existence of large TE–TM polarization splitting in the open-access microcavity

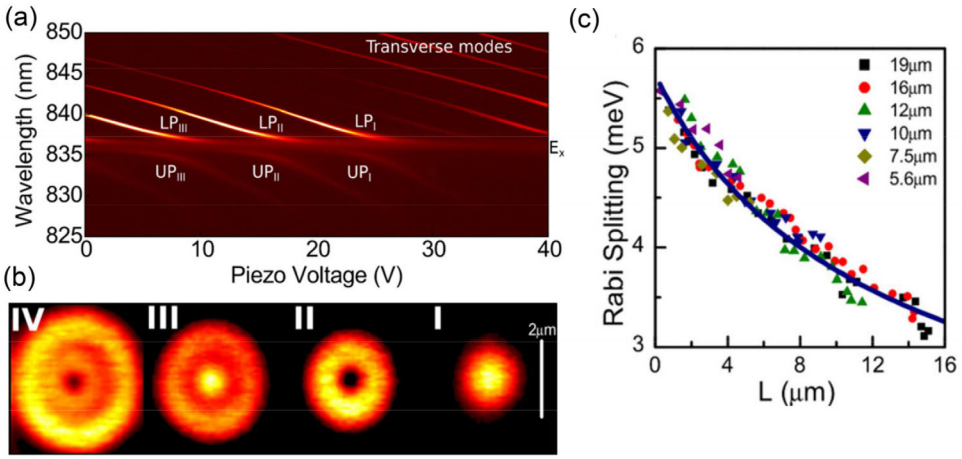

Figure 8. Characterization of the strong coupling regime in a chip-based open-access microcavity with InGaAs QWs. a) Anticrossing feature that evidences the strong exciton–photon coupling. LP/UP$_i$ refers to the lower/upper polariton of the ith transverse Gaussian mode. b) Real space photoluminescence (PL) image of the transverse Gaussian modes. c) Rabi splitting as a function of cavity length L with different RoCs ranging from 5.6 to 19 μm. Reproduced with permission.[46] Copyright 2014, AIP Publishing.

renders it a unique system of photonic spin–orbit (SO) coupling. Indeed, for 2D polaritons created in planar microcavities, the TE–TM splitting acts as an effective magnetic field on cavity photons, leading to interesting phenomena such as optical spin Hall effect,[67] magnetic-monopole-like half dark solitons,[88] and polaritonic topological insulators.[8,9,69] Dufferwiel et al. reported polariton condensates exhibiting vortex-like pseudospin textures in a chip-based open-access microcavity.[89] A combined effect of the confinement potential created by the concave mirror and the spin–orbit coupling induced by the large TE–TM splitting results in a lifting of degeneracy of the first excited manifold (corresponding to LG mode with $(p, |l|) = (0, 1)$), showing eigenstates of radial/azimuthal spin vortices and hyperbolic-like spin antivortices (**Figure 9**a). The second manifold (corresponding to the degenerated LG modes $(p, |l|) = (1, 0)$ and (0,2)) also splits under the SO coupling effect, showing different ways of pseudospin winding in the inner core and outer ring of the same mode (Figure 9b). The effect of strong light–matter coupling was investigated in such systems by modifying the exciton/photon fraction, depending on which the polaritons choose to condense either in spin-vortex-like patterns or linearly polarized HG states.[89] Compared to other polaritonic systems exhibiting spin vortices,[86,90] the open-access microcavity shows its capability of creating spin vortices in a controllable way, as well as the in situ tunability of spin textures by involving the polaritonic properties.

The observation of spin vortices confirms the possibility to use open-access microcavities as a system for manipulating the spin–orbital coupled states of photons. Li et al. proposed a protocol for such manipulation in a spin–orbit coupled Poincare hypersphere, using the polarization-dependent AC Stark effect of excitons under ultrafast pump pulses.[91]

3.2.3. Polaritonic Molecules

The design of partially overlapped hemispheres as concave mirrors in chip-based open-access microcavities, sketched in **Figure 10**a, was introduced to exciton-polariton studies by Dufferwiel et al. in 2015, forming polaritonic molecules exhibiting bonding (B) and antibonding (AB) eigenstates.[50] The major difference between the polaritonic molecules reported in the work and other systems lies in the tunability of the mode coupling strength by varying the photon fractions. Since the mode coupling that leads to the B–AB mode splitting is a pure photonic effect, the splitting vanishes when the polaritons approach the exciton energy presenting very small photon fraction, as shown in Figure 10b. The tunability of individual cavities is a major advantage compared to polaritonic molecules based on monolithic microcavities.[92] By changing the tilt angle of the planar cavity mirror, the relative length difference between the two coupled cavities can be tuned precisely, depending on which the cavity modes can be coupled and decoupled. The structure of polaritonic molecule has been proposed as a promising system for demonstrating unconventional polariton blockade sketched in Figure 7b, in which the required polariton nonlinearity reduces via the effect of quantum tunneling between the two coupled cavities.[93,94] Meanwhile, the flexible shape design of the coupled open-access microcavity is also promising to serve as a suitable experimental platform for investigating the non-Hermitian physics and quantum photon transport introduced in Section 3.1.2.

3.2.4. Quantum Correlation of Polaritons

For experimental investigations of polariton quantum correlations with open-access microcavities, the pump photons are usually provided by a laser that is near resonant with the polariton energy. In order to distinguish the emission of cavity polaritons from the backscattered pump laser, the best solution is to structure the setup in transmission configuration as discussed in previous sections (Figure 4a,c). The realization of such transmission setup at liquid helium temperature is reported in a number of works from both fiber- and chip-based cavities.[41,42,95]

Optical Bistability and Dissipative Phase Transition: When the pump laser is at a proper range of blue detuning with respect

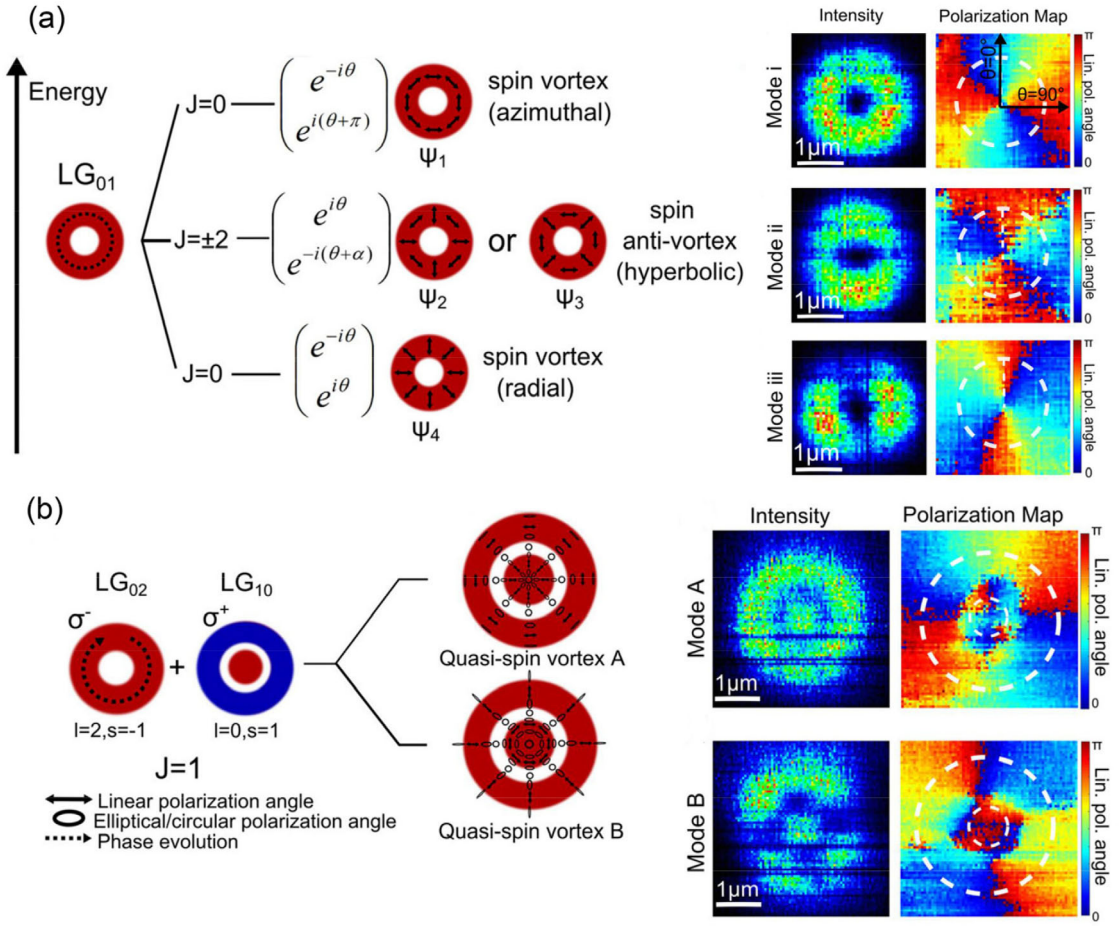

Figure 9. Polaritonic spin vortices. a) For the first excited manifold: schematic of the formation of the eigenstates of radial/azimuthal spin vortices and hyperbolic-like spin anti-vortices (left panel) and the corresponding experimental results including spatially resolved PL intensity and linear polarization angle distribution (right panel). b) Same as (a) for the second excited manifold. Reproduced with permission.[89] Copyright 2015, APS.

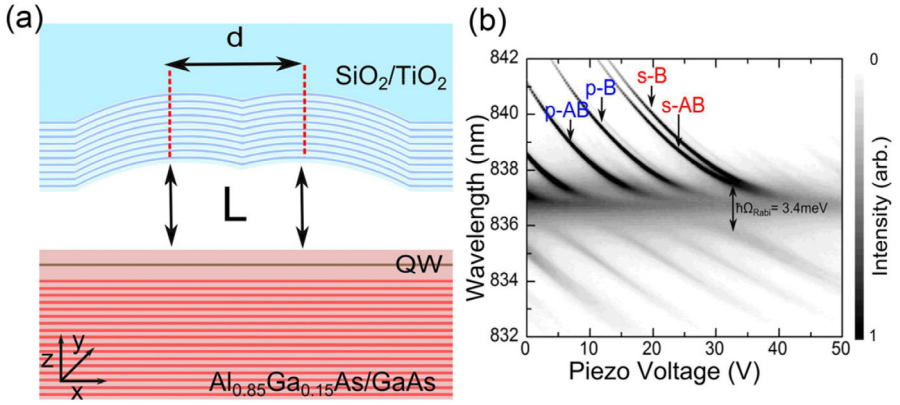

Figure 10. Polaritonic molecules based on open-access microcavities. a) Schematic of the cavity configuration. b) Anticrossing feature of the B and AB modes, whereas the B–AB splitting vanishes when approaching the exciton energy. Reproduced with permission.[50] Copyright 2015, AIP Publishing.

to the polariton energy, optical bistability of polaritons, featured by the coexistence of two stable states, occurred within a certain range of pump power in polaritonic systems due to nonlinear interactions.[96]

As strongly linked to the open dissipative nature and quantum properties of polariton systems, optical bistability has been explored both experimentally and theoretically as a lasting focus of polariton physics in monolithic microcavities. In 2008, Krizhanovskii et al. observed experimentally that under CW (continuous wave) pumping near the inflection point of the polariton dispersion, sharp transformations of polariton–polariton scattering patterns occur in momentum space with increasing pump

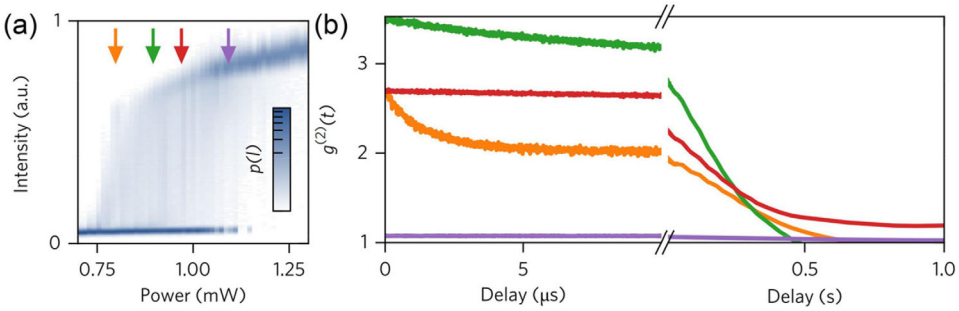

Figure 11. Optical bistability and dissipative phase transition. a) Color-coded photon number distribution showing double-peaked feature within excitation power from 750 and 1200 μW, indicating optical bistability. b) Prolonged bunching timescale up to microseconds in the bistability region is observed. The orange, green, red, and purple colors correspond to the detuning $\Delta/\gamma = 0.2$, 0.4, 0.8, and 1.0. Reproduced with permission.[41] Copyright 2018, Springer Nature.

intensity.[97] These results were well explained by the theoretical model that the interplay between the self-instability (bistability) of the pumped mode and its multimode parametric instability results in a dynamically self-organized optical parametric oscillation (OPO) process.[97,98] Demenev et al. performed time-dependent studies of the kinetics of the polariton system under nanosecond-long pump pulses, which provided direct experimental evidence for the robustness of the theoretical model.[98] In 2010, Sarkar et al. observed polarization bistability and the resultant spin-ring patterns of the polariton signal state, revealing the effect of the spin-dependent anisotropy of polariton–polariton interactions.[99] By pumping near the inflection point of polariton dispersion in the bistability regime, bright solitons and soliton trains of polaritons were created by Sich et al. in 2012 and Chana et al. in 2015.[62,100]

Similar to monolithic microcavities, optical bistability can be clearly demonstrated due to the strong nonlinearity in the open-access microcavities. Giriunas et al. reported in a chip-based open-access microcavity the formation of macroscopically occupied polariton ground state by driving a discrete excited state near-resonantly, where the polariton optical bistability of the pump state is directly inherited by the ground state of polariton condensation, showing a total number of polaritons of ≈110.[42]

The dissipative and quantum features of polaritons at the optical bistability region was investigated by Fink et al. in a fiber-based open-access microcavity, where the photon correlation measurement is demonstrated as an effective tool for studying the dynamics of dissipative phase transitions.[41] At the bistability region (**Figure 11**a), the intermittent light bursts due to the jump from low to high intensity states give rise to strong super-Poissonian photon statistics, resulting in highly bunched polariton states exhibiting a second-order correlation function $g^{(2)}(0)$ more than 2.[28] The timescale of the bunching corresponds to the relaxation time of the system back to its steady state, which is the inverse of the real part of the Liouvillian eigenvalues.[101] A dissipative quantum phase transition occurs when the Liouvillian gap closes, characterized by a critical slowdown of the relaxation timescale and thereby an extended persisting time of polariton bunching. This links the polariton correlation to the dynamics of the dissipative phase transition. At the pump laser detuning of $\Delta = +1.5\gamma$ (γ is the polariton linewidth), the authors observed prolonged bunching timescale up to microseconds in the bistability region (Figure 11b), more than nine orders of magnitude as that of single polaritons. A systematic investigation of the bunching timescale around the critical pump power (where the longest bunching timescale is obtained) reveals the reduction of the Liouvillian gap and the signature of the dissipative phase transition.

Toward Polariton Blockade: The quantum correlation of a polaritonic system when the two-particle interaction and polariton linewidth are comparable is depicted in **Figure 12**a, which shows a strong dependence of polariton statistics on the detuning of the incident laser within the polariton linewidth. If the pump laser is in resonance or slightly red-detuned with the polariton transition, the probability of creating two polaritons within the polariton lifetime is reduced due to the energy blueshift induced by polariton nonlinearity, leading to antibunching polariton states. Conversely, if the pump laser is blue-detuned with the polariton transition, the probability of simultaneously creating two polaritons is increased, resulting in polariton states of quantum bunching. Consequently, the photon correlation $g^{(2)}(0)$ presents a dispersive feature around unity (Figure 12b).[102] Muñoz-Matutano et al. reported photon correlation measurements at several laser detunings based on such scenario in a fiber cavity near-resonantly pumped by a pulsed laser. The key feature is the observation of sub-Poissonian photon statistics characterized by $g^{(2)}(0) = 0.93 \pm 0.04$.[102] The authors attributed the noise sources that partially spoil the photon correlation to the charged exciton transition and the neighboring fundamental cross-polarized polariton mode, which was minimized by tuning the system parameters. In the meantime, Delteil et al. also reported antibunching of polaritons in a fiber cavity under CW pumping by choosing an exciton fraction $|c_x|^2 \approx 0.6$ as theoretically expected to reach the optimal compromise between the polariton linewidth and nonlinearity, characterized by a $g^{(2)}(0) = 0.95 \pm 0.02$ at a negative pump detuning $\Delta = -0.75\Gamma_p$ (Γ_p is the polariton linewidth).[103] These results enlightened the way toward polariton quantum blockade that would exhibit greatly reduced $g^{(2)}(0)$, probably by further narrowing the polariton linewidth with higher-quality QWs and increasing the polariton interaction with dipolar polaritons in coupled QWs.

3.3. Exciton-Polaritons from Monolayer TMDs in Open-Access Microcavities

TMDs, such as WS_2, MoS_2, WSe_2, and $MoSe_2$, is family of materials whose monolayers form direct bandgap semiconductors

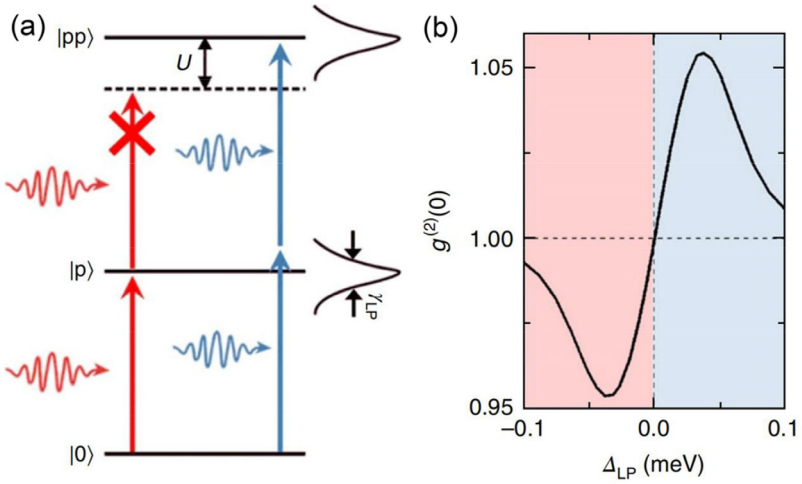

Figure 12. Quantum correlation of a polaritonic system when the energy shift of two-polariton interaction exceeds the polariton linewidth. a) The schematic of excitation mechanism and b) simulated results of second-order correlation $g^2(0)$ as a function of the pump laser–polariton detuning, with simulation parameters in ref. [102]. If the pump laser is red-detuned with the polariton transition, polariton blockade occurs (red in (a)) resulting in antibunching photon statistics (red part in (b)). If the pump laser is blue-detuned, the polariton system is preferably excited to two-particle states (blue in (b)), leading to photon bunching (blue part in (b)). Reproduced with permission.[102] Copyright 2019, Springer Nature.

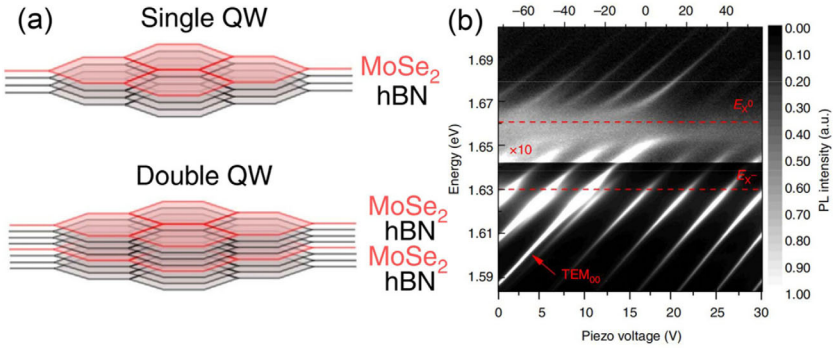

Figure 13. Strong coupling in $MoSe_2$ monolayers. a) Schematics of heterostructures of the double and single QW. b) Anticrossing feature between the monolayer exciton and cavity mode energies. Reproduced with permission.[109] Copyright 2015, Springer Nature.

exhibiting pronounced exciton resonance at room temperature due to large exciton binding energy and oscillator strength.[104–106] The strong coupling between such monolayers and microcavity photons has been attracting a lot of interest as a novel system for room temperature polaritonic devices that may also help to understand and influence the underlying electronic properties of the TMD monolayers. While the monolayers can be obtained by exfoliation and transferred to a DBR with standard transfer techniques, the deposition of a second DBR of high quality on top is the main difficulty for achieving a high-quality microcavity. Although strong coupling has been reported in a fully dielectric monolithic microcavity,[107] the cavity quality factor as well as the polariton lifetime remains low. In this sense, the use of open-access microcavities became the best solution.

3.3.1. Strong Coupling Regime

In 2014, Schwarz et al. managed to place thin sheets of GaSe in a chip-based open-access microcavity and demonstrate enhanced spontaneous emission rate.[108] The demonstration of strong coupling regime was reported by Dufferwiel et al., from the same affiliation, with $MoSe_2$ monolayers at a temperature of 4 K in 2015.[109] The vacuum Rabi splitting was observed to be 20 meV for a single $MoSe_2$ monolayer (**Figure 13**), and 29 meV in a heterostructure of $MoSe_2$/hBN/$MoSe_2$ double monolayer, in agreement with the theoretically expected scaling that the Rabi is proportional to the square root of QW numbers. A narrow polariton linewidth of 4.9 meV was achieved at zero photon–exciton detuning due to the increased cavity quality. In 2016, Flatten et al. demonstrated strong coupling regime at room temperature with WS_2 monolayers in a chip-based planar–planar open-access microcavity in 2016,[110] showing a vacuum Rabi splitting of 70 meV.

3.3.2. Valley Coherent Polaritons

The use of open-access microcavities allows to explore and modify the intrinsic electronic properties of the monolayer material, best exemplified by the demonstration of valley addressable polaritons in $MoSe_2$ monolayers by Dufferwiel et al. in 2017.[111] It had been demonstrated in earlier literature that upon

nonresonant excitation with circularly polarized light, the bare excitons in $MoSe_2$ monolayers almost does not retain the polarization of the pumped valley state, due to the Maialle–Silva–Sham (MSS) mechanism[112–114] that a combined effect of the parallel and perpendicular (LT) spin splitting of exciton states and the random exciton momentum scattering results in a valley pseudospin relaxation. Nevertheless, upon the formation of exciton-polaritons in open-access microcavities, the expected valley depolarization by MSS mechanism is reduced, due to a decrease of random exciton momentum scattering by the fact that the spatial extension of polariton wavefunction is much larger than the length scale of the exciton disorder. The authors observed polarization retention of exciton-polaritons with circular polarization degree up to 20%, compared to 2% and 5% for bare neutral and charged excitons.[111] Furthermore, the authors reported valley coherent exciton-polaritons in WSe_2 embedded in an open-access microcavity in 2018.[115] It was demonstrated that the exciton-polaritons exhibited a linear polarization degree, initiated by the nonresonant excitation of valley pseudospin, up to three times higher than bare excitons. By applying a magnetic field of 8 T, the polarization angle of the polaritons rotates up to 45% degree under the induced Zeeman effect, three times larger than the bare exciton, demonstrating a longer coherence lifetime. These results initiated a way to use valley coherence for on-chip photonic devices.

3.3.3. Fermi Polaron-Polaritons

The use of open-access microcavities allows to combine advantageous properties of the TMD monolayer and the cavity, of which the Fermi polaron-polariton is a typical example. The concept of polaron was initially described by the interaction of an atomic or trion with surrounding electrons.[116] In semiconductors, polarons are formed by the exciton–electron interaction, in which an optically created exciton serves as a mobile bosonic impurity in a fermionic reservoir of electrons. Electrons can be either attracted or pushed away by the exciton, resulting in attractive and repulsive polaron states split in energy. Sidler et al. investigated polaron-polaritons formed by the strong coupling between microcavity photons and polarons in a $MoSe_2$ monolayer.[117] The monolayer with metal contact allows free tuning of electron density which is a deterministic factor of polaron properties, whilst the fiber cavity allows easy cavity–monolayer integration and transmission spectroscopy with white light. The authors observed repulsive and attractive polarons in both weak and strong coupling regimes, the energies of which shifted with electron density. Similar to the exciton-polariton which can exhibit an effective mass four orders of magnitude smaller than the electrons, the polaron-polariton is promising for the realization of Fermi-polaron systems with tunable ultrasmall mass impurity.

3.4. Exciton-Polaritons and Photon Condensates in Organic Materials in Open-Access Microcavities

3.4.1. Organic Semiconductors

Organic semiconductors, being polymers or small-molecule-consisted microcrystals, are a new type of semiconductors hosting Frenkel excitons that exhibit very large binding energy ($\approx$1 eV) and oscillator strength (hundreds of millielectronvolts), suitable for polaritonic devices at room temperature.[118,119] Strong coupling and polariton condensation based on various organic materials have already been reported in monolithic microcavities despite the low Q-factor around several hundreds.[120,121] The limiting factor for further increasing the cavity Q and thus the polariton lifetime lies in the technical difficulty of depositing high-quality DBRs on top of the polymer surface, which can be hopefully settled with open-access microcavities. In 2016, Urbonas et al. demonstrated strong exciton–photon coupling between a ladder-type conjugated polymer and a chip-based open-access microcavity at room temperature, showing a Q-factor of 200 and vacuum Rabi splitting of 166 meV.[122] The authors also demonstrated polaritonic molecules by applying coupled hemispherical mirrors. In 2017, the same research group demonstrated polariton condensation with the same polymer and the cavity Q-factor improved to 600.[123] In addition, Betzold et al. reported strong exciton–photon coupling of a fluorescent emitter (MEH-PBI) embedded in a chip-based open-access microcavity in 2017.[124] The authors observed a transition from weak to strong coupling regimes by decreasing the cavity length through several longitudinal orders. The open-access microcavities also allow to study optical behaviors of biological related chemicals. As an example, Grant et al. investigated a thin film of biologically derived molecule β-carotene embedded in a planar–planar open-access microcavity with silver-coated cavity mirrors.[125] The strong coupling was demonstrated between the cavity mode and the 0–1 vibronic transition of the molecule, but not for other vibronic transitions due to their lower oscillator strengths and broader linewidths.

3.4.2. Dye Lasers and Photon Condensations

Organic dye molecules in solutions have been popularly used as active media for various lasers covering a wide range of wavelengths.[126] Nevertheless, due to the irreversible photobleaching of dye molecules, conventional organic dye lasers require either large-sized pump circulation system or pulsed pumping with external sources. Coles et al. reports a solution to these drawbacks by incorporating dye molecules inside a chip-based open-access microcavity.[127] The small mode volume of the system allows self-diffusion that quickly circulates photobleached dye molecules out of the cavity mode, in which the authors demonstrated CW operation of a dye laser without externally driven recirculation, with single mode tunability over a bandwidth of 20 nm. In parallel with dye-based microlasers, dye molecules incorporated in cavities were also investigated for photon condensations, wherein the photons can reach thermal equilibrium through frequent energy exchanges with the thermal bath of dye–solvent vibrations.[128–132] Walker et al. reported nonequilibrium BEC of a very small number (7 ± 2) of photons in the chip-based open-access microcavity incorporating dye molecules.[133] The concave mirror, with a RoC of 400 μm fabricated by FIB milling, was specifically designed to form a photonic potential of 2D harmonic oscillator that enabled the observation of a multimode condensate regime of photons that exhibit strong intermode correlations.

4. Single-Photon Emitters and Nanoparticles in Open-Access Microcavities

Solid-state single-photon emitters, including QDs,[95] vacancy color centers,[134] single molecules,[45] provide atomic-like two-level systems by the nanoscale confinement of charge carriers that enable significant applications for on-chip quantum information processing.[135] The investigation of cavity quantum electrodynamics (CQED) by integrating single-photon emitters in microcavities allows tailoring the light–matter interaction,[136] leading to enhanced spontaneous emission rate via the Purcell effect,[137] higher photon collection efficiency,[18] better photon purity and indistinguishability,[138] as well as photon–spin interfaces.[139] Moreover, the interaction of single-photon emitters with cavity photons or other coupling media would enable the entanglement between remote qubits, for which various protocols have been proposed. Imamoglu et al. proposed a scheme for achieving entanglement between distant QD electron spins coupled through a common microcavity mode using all-optical Raman transitions.[140] Alternatively, Yokoshi et al. proposed a scheme to create entangled distant qubits of heavy hole spin in QDs through a spontaneously radiated cavity photon that travels via a waveguide strongly coupled with the two cavities in which the QDs are located.[141] More recently, Maslova et al. proposed a protocol to increase spin correlations and the degree of entanglement in a system of two correlated QDs by coupling it to an electronic reservoir, which is explained by the collective behavior of all electrons linked to the symmetry properties of the whole system.[142]

The key technical issue to guarantee the most efficient emitter–cavity coupling is to ensure the optimal spatial and temporal overlaps, that is, the emitter needs to be located at the very center of the optical field maximum and the transition exhibits the same optical frequency with the cavity mode. Although numerous techniques have been developed to improve the overlap in monolithic cavities such as QD position registration,[143,144] temperature,[145] and electrical tuning of excitonic energy,[146,147] it is still challenging to achieve prefect alignments without deteriorating the optical properties of the emitter. In this context, open-access microcavities are expected as a versatile tool for a perfect photon–emitter overlap without any manipulation on the emitter itself. Indeed, the cavity can be continuously tuned to perfect overlaps with the emitter in space and frequency domains by simply adjusting the lateral position of the concave mirror and the cavity length respectively. Such in situ tunability has been a strong motivation for the successive advancement of open-access microcavity systems.

4.1. Semiconductor QDs in Open-Access Microcavities

4.1.1. Epitaxial QDs

The self-assembled InGaAs or InAs QDs are the most widely studied epitaxial QDs, which are grown by epitaxy on an epitaxial AlGaAs/GaAs DBR that serves as the planar mirror of the open-access microcavity.[95] Muller et al. first reported the coupling of single InGaAs QD with a fiber-based open-access microcavity (RoC ≈42 µm) in 2009.[36] By varying the cavity length, the cavity mode which crossed the resonances of different QD transitions showed enhanced intensity of emission (**Figure 14**a). In 2011, Barbour et al. realized cavity-QD resonance in a chip-based open-access microcavity with a RoC ≈120 µm, in which the Purcell effect evidenced by enhanced spontaneous emission rate was observed.[27] In order to enhance the coupling strength with smaller mode volume, Greuter et al. from the same group improved fabrication process of the laser ablation that allows to

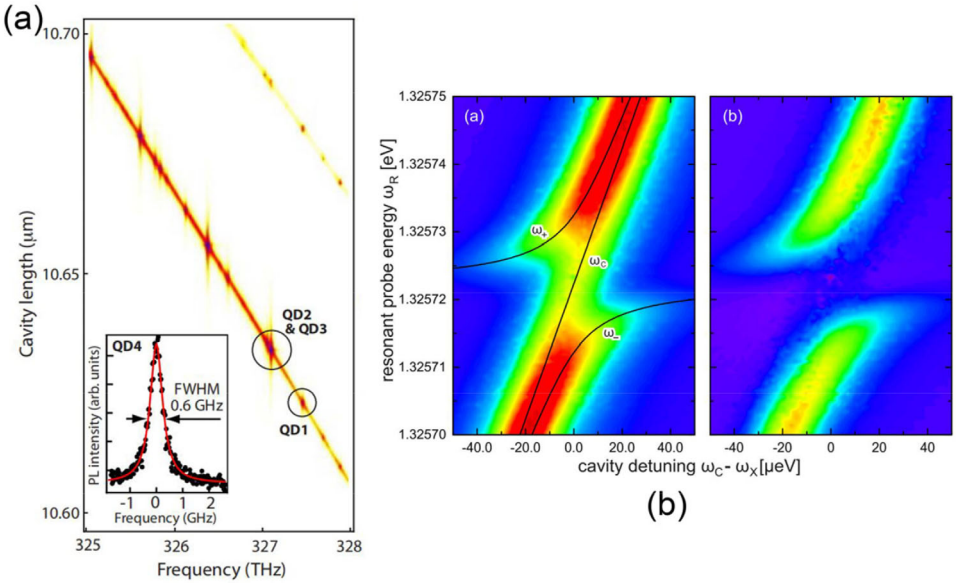

Figure 14. Coupling between epitaxial QDs and open-access microcavities. a) The weak coupling regime: PL spectra of microcavity with varying cavity length. Reproduced with permission.[36] Copyright 2009, AIP Publishing. b) The strong coupling regime: anticrossing behavior when tuning the cavity mode energy through the QD, raw data (left panel), and data subtracting the bare-cavity resonance (right panel). Reproduced with permission.[95] Copyright 2015, APS.

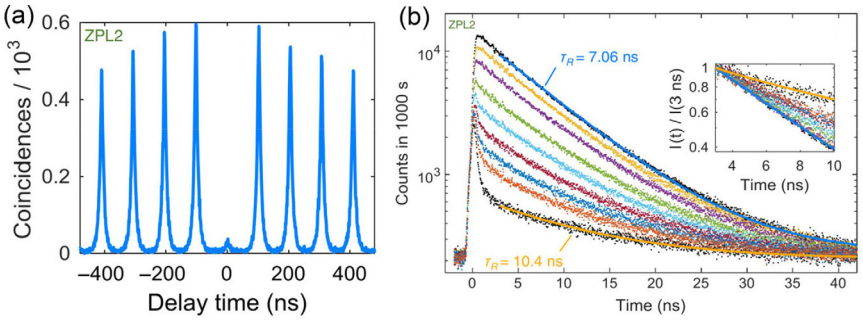

Figure 15. NV centers in diamonds integrated in open-access microcavities. a) $g^{(2)}(t)$ measurement showing the evidence of the single-photon emission. b) PL decay curves with pulsed excitation as a function of cavity-length detuning. The inset shows the normalized decay curves. Reproduced with permission.[159] Copyright 2017, APS.

reduce the RoC of the concave cavity mirror to 10 µm.[38,148] The authors reported strong coupling between a single QD and the cavity evidenced by the observation of the anticrossing behavior when tuning the cavity mode energy to the QD transition (Figure 14b), with enhanced cooperativity allowed by the high quality of the spectra.[95]

4.1.2. Nanocrystal QDs

Nanocrystal QDs are widely used for light-emitting devices, single-photon sources, and lasers. As the emission wavelength depends on the size of individual synthetized QDs, the integration of such emitters with the open-access microcavity provides flexible tunability for accurate photon–emitter coupling and laser wavelength tuning. In 2012, Di et al. reported the control of spontaneous emission of CdSe/ZnS nanocrystals in a chip-based open-access microcavity at room temperature.[149] While the system worked in the "bad emitter" regime in which the QD transition linewidth is much greater than the cavity linewidth due to dephasing, the ultrasmall mode volume becomes the key factor for achieving enhanced spontaneous emission. The authors measured spontaneous emission rate for a series of mode volumes at different RoCs of cavity mirrors, showing greater enhancement observed with reducing mode volumes. In 2016, Patel et al. reported tunable single mode lasing within a broad range of wavelength over 25 nm in a system of CdSe/CdS core–shell nanocrystals in a chip-based open-access microcavity, based on which gain spectroscopy of the QD solution was demonstrated.[150]

4.2. NV Centers in Diamonds in Open-Access Microcavities

The nitrogen vacancy (NV) centers in diamonds have been intensively investigated for quantum information processing due to its long spin coherence time and robust single-photon emission.[134,151,152] Microcavities are commonly used as the main platform for embedding the NV center for high generation rate and collection efficiency of indistinguishable single photons, as well as for enhancing the zero-phonon-line (ZPL) emission of the NV center at room temperature. The integration of NV centers has been successfully demonstrated in WGM and 2D photonic crystal (PhC) cavities,[153–155] however, it remains challenging to fabricate a NV center-embedded microcavity with both small mode volume and highly directional emission. The open-access microcavity provides a realistic solution with in situ tunability, while the NV centers can be made onto the planar DBR by either spin casting nanodiamonds or transferring a single crystalline diamond membrane. In 2015, Johnson et al. reported the integration of nanodiamonds in a chip-based open-access microcavity, allowing 6.25 times of ZPL emission intensity compared to bare NV centers at room temperature.[156] Dolan et al. demonstrated in the same type of cavity single-photon generation, which exhibited photon purities exceeding 96% and device efficiencies up to 3%.[157] The authors also carried out systematic studies using concave mirrors with a series of RoCs ranging from 4 to 25 µm, and concluded that RoC = 8 µm enabled the best device performance by the interplay between cavity feeding and photon extraction. With fiber-based cavities, Kaupp et al., demonstrated Purcell enhancement up to two of NV centers in nanodiamonds in 2016.[158] In 2017, Riedel et al. reported the integration of diamond membranes, detached from the hosting substrate using a micromanipulator, with a chip-based open-access microcavity.[159] The authors reported single-photon emission (**Figure 15**a) and claimed a Purcell factor of ≈30 for the ZPL translated from an overall Purcell factor of 2 (Figure 15b). Within the cavity, the probability of the ZPL emission was increased to 46% compared to 3% for bare NV. Bogdanovic et al. reported a fabrication process to include microwave stripes on the planar mirror of a fiber-based open-access microcavity embedded with diamond membranes in 2017, which enables the demonstration of NV spin control with microwaves.[160]

4.3. Single Molecules in Open-Access Microcavities

Single molecules have been reported as single-photon emitters whilst their strong coupling with photons were demonstrated in plasmonic nanostructures.[161,162] Nevertheless, the realization of selectively addressing the narrow linewidth transitions in single molecules requires high-Q photonic devices like microcavities. The tunability, easy integration, small volume, and high Q of the open-access microcavity system render it an excellent candidate for hosting single molecule emitters. The single molecule microcavity-integrated systems were most developed by researchers at Max Planck Institute for the Science of Light at Erlangen, Germany. Following the initiation and improvement of

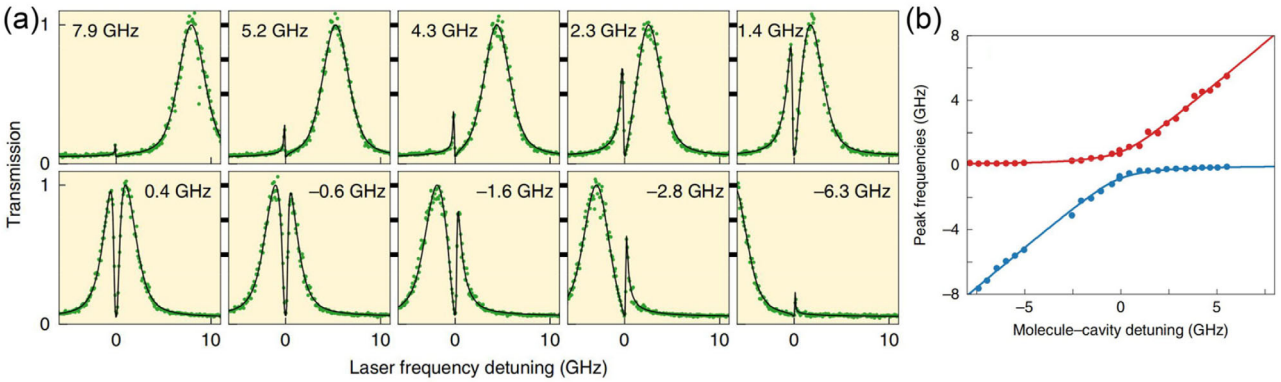

Figure 16. Strong coupling between a single molecule exciton and a tunable open-access microcavity. a) Spectra obtained by varying cavity–molecule frequency detuning. b) The corresponding anticrossing feature characterized by the measured peak frequency as a function of molecule-cavity detuning. Reproduced with permission.[45] Copyright 2019, Springer Nature.

the cavity samples in 2010[163] and 2015,[43] Wang et al. demonstrated in 2017 the coherent coupling of a single dibenzoterrylene (DBT) molecule with an open-access microcavity consisting of a DBR-coated planar mirror and a metal-coated concave mirror on silicon substrate.[164] The cavity exhibits a moderate Q-factor of ≈1500 that is high enough to allow 66% enhancement of the 00ZPL at cryogen temperature and low enough to avoid the need of extra cavity stabilization. The authors reported a 38% extinction ratio of the cavity photons by the DBT molecule within a very narrow linewidth of 54 MHz and a series of spectra showing dispersive Fano resonances at various cavity–molecule frequency detunings. In 2019, Wang et al. further improved the cavity quality by using a DBR-coated concave mirror fabricated on a fiber facet while introducing active cavity stabilization (already discussed in Section 2.3.5), leading to a very high Q factor of 230 000. Such a sophisticated system allows to turn the single DBT molecule into a coherent two-level quantum system.[45] By continuously varying cavity–molecule frequency detuning, the authors observed the evolution of spectra showing two split polaritonic resonances (**Figure 16**a), evidencing the strong coupling regime of a single molecule with the optical microcavity by the anticrossing feature of photon energy (Figure 16b). Moreover, the authors reported one of the largest photon bunching of $g^{(2)}(0) = 21$ for single emitters that is related to the high cooperativity of the strongly coupled system. The authors also demonstrated the efficient interaction of the molecule-in-cavity system with single photons from another molecule in a distant laboratory, thereby "wiring" a single photon to a single quantum emitter.

4.4. Nanoparticle Trapping and Sensing in Open-Access Microcavities

Microcavities are well known to be used as sensors for nanoparticles, chemical gases, temperatures, magnetic fields, and small mechanical forces, characterized by the effects of spectral shifting, splitting, and broadening of the cavity optical modes due to the existence of the sensed object or parameter change.[165–168] Moreover, enhancement of optical field inside microcavities are used to optically trap nanoparticles.[44] Open-access microcavities were recently applied for enhancing the sensing and trapping of nanoparticles with small mode volumes. In 2014, Trichet et al. developed a system of custom-made flow cell to allow fluid between the cavity mirrors of the open-access microcavity, and reported high sensitive refractive index sensing.[169] Further in 2016, the authors introduced PMMA nanoparticles in such a system and demonstrated trapping and sensing of a single nanoparticle.[44] When a trapping event occurred, the spectrum shows an obvious mode frequency shift with significant fluctuations due to the Brownian motion of the trapped particle, which was analyzed to show the ability to determine the nanoparticle polarizability and coefficient of friction. In 2015, Kelkar et al. reported nanoparticle sensing in an open-access microcavity with gold-coated concave mirrors fabricated on a cantilever, whilst the sensed gold nanoparticles were spin coated on the bottom DBR mirror.[43] Optical mode frequency and linewidth were measured and mapped, exhibiting variation at the position of the nanoparticle. Interestingly, the authors observed mode linewidth narrowing instead of broadening by the embedded nanoparticle at long cavity lengths, which was explained by the fact that the nanoparticle could reduce the power scattered outside the cavity of specific structures.

5. Conclusion and Outlook

The tunable open-access microcavity provides a versatile platform for investigating light–matter interactions in a broad range of research areas, due to its precise tunability, small mode volume, flexibility of design, and easiness for integration with emitters. Whilst it has been most intensively used for polaritonics, quantum emitters, and sensing at the current stage, new applications have also been appearing such as Purcell enhanced Raman scattering[170] and enhanced light absorption in superconducting nanowire single-photon detectors.[171] Standing on the basis of the reported achievements, further advances of potential applications of open-access microcavities are expected in the near future. The freedom of structural design will allow optimal integration of surface-plasmonic nanostructures into dielectric microcavities, whereas the coupling between the plasmonic and optical modes leads to a combination of high Q-factor and nanoscale mode volume, further enhancing the light–matter interaction of single emitters coupled to such hybrid modes.[172–174] It is highly

expected that the spatial and spectral tunability could enable the most optimized emitter–cavity matching, resulting in even higher single-photon extraction efficiency than the micropillar-based cavities,[18,138,139] a crucial need for photon-based quantum computing processes such as the boson sampling.[175,176] By entering the strong coupling regime with tunable cooperativity, photon trains of on-demand quantum bunching could be realized.[45,177,178] Another merit of open-access microcavities that should not be ignored is the higher-order transverse modes carrying OAM which, if integrated with quantum emitters, might be essential for realizing qubits with high degrees of freedom.[179–181] For the investigation of collective behavior of photons and polaritons, the flexible shape design of the concave mirror with high accuracy allowed by the FIB milling gives rise to the advantage of sculpturing photonic potentials. For example, a parabolic photonic potential could be defined to support a series of exactly equally spaced eigenenergy levels that might be used to realize bosonic cascade lasers.[182] Moreover, photonic superlattices of topological structures could be realized with coupled arrays or matrices of concave mirrors, avoiding deterioration of excitonic properties due to the etching into active materials. Last but not least, the "open-access" structure itself still exhibits great significance. it could allow external modulation of the emitter properties, such as applying surface acoustic waves (SAW), directly on the active layer instead of through the top DBR, which would lead to spatially localized exciton wavefunction with quasi-continuum energy spectrum.[46,183,184] In the long run, the "open-access" feature will always be a figure of merit to facilitate the investigation on light–matter coupling of various newly emerging optical materials that could be otherwise hard to be integrated in high-quality microcavities.

Acknowledgements

This work was supported by National Key R&D Program of China (2017YFA0303703), National Natural Science Foundation of China (11804267), and the Natural Science Foundation of Shaanxi Province (2018JQ6041).

Conflict of Interest

The authors declare no conflict of interest.

Keywords

exciton-polaritons, monolayer transition metal dichalcogenides, open-access microcavities, optical vortices, single-photon emitters

Received: June 2, 2019
Revised: July 15, 2019
Published online: August 7, 2019

[1] K. J. Vahala, *Nature* **2003**, *424*, 839.
[2] I. Carusotto, C. Ciuti, *Rev. Mod. Phys.* **2013**, *85*, 299.
[3] M. S. Skolnick, T. A. Fisher, D. M. Whittaker, *Semicond. Sci. Technol.* **1998**, *13*, 645.
[4] E. M. Purcell, H. C. Torrey, R. V. Pound, *Phys. Rev.* **1946**, *69*, 37.
[5] B. Gayral, *Ann. Phys.* (*France*) **2001**, *26*, 1.
[6] X. C. Zhang, A. Shkurinov, Y. Zhang, *Nat. Photonics* **2017**, *11*, 16.
[7] B. Kolaric, B. Maes, K. Clays, T. Durt, Y. Caudano, *Adv. Quantum Technol.* **2018**, *1*, 1800001.
[8] S. Klembt, T. H. Harder, O. A. Egorov, K. Winkler, R. Ge, M. A. Bandres, M. Emmerling, L. Worschech, T. C. H. Liew, M. Segev, C. Schneider, S. Höfling, *Nature* **2018**, *562*, 552.
[9] A. V. Nalitov, D. D. Solnyshkov, G. Malpuech, *Phys. Rev. Lett.* **2015**, *114*, 116401.
[10] Y. Li, L. Feng, F. Li, P. Hu, M. Du, X. Su, D. Sun, H. Tang, Q. Li, F. Yun, *ACS Photonics* **2018**, *5*, 4259.
[11] K. Nozaki, T. Tanabe, A. Shinya, S. Matsuo, T. Sato, H. Taniyama, M. Notomi, *Nat. Photonics* **2010**, *4*, 477.
[12] S. Hua, J. Wen, X. Jiang, Q. Hua, L. Jiang, M. Xiao, *Nat. Commun.* **2016**, *7*, 13657.
[13] Z. Shen, Y.-L. Zhang, Y. Chen, C.-L. Zou, Y.-F. Xiao, X.-B. Zou, F.-W. Sun, G.-C. Guo, C.-H. Dong, *Nat. Photonics* **2016**, *10*, 657.
[14] W. Chen, Ş. K. Özdemir, G. Zhao, J. Wiersig, L. Yang, *Nature* **2017**, *548*, 192.
[15] D. Ballarini, M. De Giorgi, E. Cancellieri, R. Houdré, E. Giacobino, R. Cingolani, A. Bramati, G. Gigli, D. Sanvitto, *Nat. Commun.* **2013**, *4*, 1778.
[16] A. Amo, J. Bloch, *C. R. Phys.* **2016**, *17*, 934.
[17] A. Aspuru-Guzik, P. Walther, *Nat. Phys.* **2012**, *8*, 285.
[18] X. Ding, Y. He, Z.-C. Duan, N. Gregersen, M.-C. Chen, S. Unsleber, S. Maier, C. Schneider, M. Kamp, S. Höfling, C.-Y. Lu, J.-W. Pan, *Phys. Rev. Lett.* **2016**, *116*, 020401.
[19] P. W. Milonni, J. H. Eberly, *Laser Physics*, Wiley, Hoboken, NJ **2010**.
[20] G. Nardin, Y. Léger, B. Pietka, F. Morier-Genoud, B. Deveaud-Plédran, *Phys. Rev. B* **2010**, *82*, 045304.
[21] H. Eleuch, J. M. Courty, G. Messin, C. Fabre, E. Giacobino, *J. Opt. B: Quantum Semiclassical Opt.* **1999**, *1*, 1.
[22] F. Li, *Ph.D. Thesis*, Université Nice Sophia Antipolis **2013**.
[23] G. Dasbach, C. Diederichs, J. Tignon, C. Ciuti, P. Roussignol, C. Delalande, M. Bayer, A. Forchel, *Phys. Rev. B* **2005**, *71*, 161308(R).
[24] M. Trupke, E. A. Hinds, S. Eriksson, E. A. Curtis, Z. Moktadir, E. Kukharenka, M. Kraft, *Appl. Phys. Lett.* **2005**, *87*, 211106.
[25] T. Steinmetz, Y. Colombe, D. Hunger, T. W. Hänsch, A. Balocchi, R. J. Warburton, J. Reichel, *Appl. Phys. Lett.* **2006**, *89*, 111110.
[26] R. C. Pennington, G. D'Alessandro, J. J. Baumberg, M. Kaczmarek, *Opt. Lett.* **2007**, *32*, 3131.
[27] R. J. Barbour, P. A. Dalgarno, A. Curran, K. M. Nowak, H. J. Baker, D. R. Hall, N. G. Stoltz, P. M. Petroff, R. J. Warburton, *J. Appl. Phys.* **2011**, *110*, 053107.
[28] T. Fink, *Ph.D. Thesis*, ETH Zürich **2018**.
[29] P. Qing, J. Gong, X. Lin, N. Yao, W. Shen, A. Rahimi-Iman, W. Fang, L. Tong, *Appl. Phys. Lett.* **2019**, *114*, 021106.
[30] P. R. Dolan, G. M. Hughes, F. Grazioso, B. R. Patton, J. M. Smith, *Opt. Lett.* **2010**, *35*, 3556.
[31] P. R. Dolan, *Ph.D. Thesis*, University of Oxford **2013**.
[32] A. A. P. Trichet, P. R. Dolan, D. M. Coles, G. M. Hughes, J. M. Smith, *Opt. Express* **2015**, *23*, 17205.
[33] A. A. P. Trichet, P. R. Dolan, J. M. Smith, *J. Opt.* **2018**, *20*, 035402.
[34] B. Besga, C. Vaneph, J. Reichel, J. Esteve, A. Reinhard, J. Miguel-sanchez, A. Imamoglu, T. Volz, *Phys. Rev. Appl.* **2015**, *3*, 014008.
[35] Y. Colombe, T. Steinmetz, G. Dubois, F. Linke, D. Hunger, J. Reichel, *Nature* **2007**, *450*, 272.
[36] A. Muller, E. B. Flagg, M. Metcalfe, J. R. Lawall, G. S. Solomon, *Appl. Phys. Lett.* **2009**, *95*, 173101.
[37] A. Muller, E. B. Flagg, J. R. Lawall, G. S. Solomon, *Opt. Lett.* **2010**, *35*, 2293.
[38] L. Greuter, S. Starosielec, D. Najer, A. Ludwig, L. Duempelmann, D. Rohner, R. J. Warburton, *Appl. Phys. Lett.* **2014**, *105*, 121105.

[39] S. Dufferwiel, *Ph.D. Thesis*, University of Sheffield, UK **2014**.
[40] D. Hunger, T. Steinmetz, Y. Colombe, C. Deutsch, T. W. Hänsch, J. Reichel, *New J. Phys.* **2010**, *12*, 065038.
[41] T. Fink, A. Schade, S. Höfling, C. Schneider, A. Imamoglu, *Nat. Phys.* **2018**, *14*, 365.
[42] L. Giriunas, F. Li, M. Sich, E. Cancellieri, R. P. A. Emmanuele, A. A. P. Trichet, I. Farrer, D. A. Ritchie, J. M. Smith, D. M. Whittaker, M. S. Skolnick, D. N. Krizhanovskii, *J. Appl. Phys.* **2018**, *124*, 025703.
[43] H. Kelkar, D. Wang, D. Martín-Cano, B. Hoffmann, S. Christiansen, S. Götzinger, V. Sandoghdar, *Phys. Rev. Appl.* **2015**, *4*, 054010.
[44] A. A. P. Trichet, P. R. Dolan, D. James, G. M. Hughes, C. Vallance, J. M. Smith, *Nano Lett.* **2016**, *16*, 6172.
[45] D. Wang, H. Kelkar, D. Martin-Cano, D. Rattenbacher, A. Shkarin, T. Utikal, S. Götzinger, V. Sandoghdar, *Nat. Phys.* **2019**, *15*, 483.
[46] S. Dufferwiel, F. Fras, A. A. P. Trichet, P. M. Walker, F. Li, L. Giriunas, M. N. Makhonin, L. R. Wilson, J. M. Smith, E. Clarke, M. S. Skolnick, D. N. Krizhanovskii, *Appl. Phys. Lett.* **2014**, *104*, 192107.
[47] R. C. Pennington, G. D'Alessandro, J. J. Baumberg, M. Kaczmarek, *Phys. Rev. A* **2009**, *79*, 043822.
[48] J. Benedikter, T. Hümmer, M. Mader, B. Schlederer, J. Reichel, T. W. Hänsch, D. Hunger, *New J. Phys.* **2015**, *17*, 053051.
[49] L. C. Flatten, A. A. P. Trichet, J. M. Smith, *Laser Photonics Rev*. **2016**, *10*, 257.
[50] S. Dufferwiel, F. Li, A. A. P. Trichet, L. Giriunas, P. M. Walker, I. Farrer, D. A. Ritchie, J. M. Smith, M. S. Skolnick, D. N. Krizhanovskii, *Appl. Phys. Lett.* **2015**, *107*, 201106.
[51] D. Kleckner, W. T. M. Irvine, S. S. R. Oemrawsingh, D. Bouwmeester, *Phys. Rev. A* **2010**, *81*, 043814.
[52] A. V. Kavokin, J. J. Baumberg, G. Malpuech, F. P. Laussy, *Microcavities*, Oxford University Press, Oxford **2017**.
[53] C. Weisbuch, M. Nishioka, A. Ishikawa, Y. Arakawa, *Phys. Rev. Lett.* **1992**, *69*, 3314.
[54] R. Balili, V. Hartwell, D. Snoke, L. Pfeiffer, K. West, *Science* **2007**, *316*, 1007.
[55] J. Kasprzak, M. Richard, S. Kundermann, A. Baas, P. Jeambrun, J. M. J. Keeling, F. M. Marchetti, M. H. Szymańska, R. André, J. L. Staehli, V. Savona, P. B. Littlewood, B. Deveaud, L. S. Dang, *Nature* **2006**, *443*, 409.
[56] K. G. Lagoudakis, M. Wouters, M. Richard, A. Baas, I. Carusotto, R. André, L. S. Dang, B. Deveaud-Plédran, *Nat. Phys.* **2008**, *4*, 706.
[57] G. Nardin, G. Grosso, Y. Léger, B. Pięt̨ka, F. Morier-Genoud, B. Deveaud-Plédran, *Nat. Phys.* **2011**, *7*, 635.
[58] D. Sanvitto, S. Pigeon, A. Amo, D. Ballarini, M. De Giorgi, I. Carusotto, R. Hivet, F. Pisanello, V. G. Sala, P. S. S. Guimaraes, R. Houdré, E. Giacobino, C. Ciuti, A. Bramati, G. Gigli, *Nat. Photonics* **2011**, *5*, 610.
[59] A. Amo, J. Lefrère, S. Pigeon, C. Adrados, C. Ciuti, I. Carusotto, R. Houdré, E. Giacobino, A. Bramati, *Nat. Phys.* **2009**, *5*, 805.
[60] A. Amo, D. Sanvitto, F. P. Laussy, D. Ballarini, E. Del Valle, M. D. Martin, A. Lemaitre, J. Bloch, D. N. Krizhanovskii, M. S. Skolnick, C. Tejedor, L. Viña, *Nature* **2009**, *457*, 291.
[61] A. Amo, S. Pigeon, D. Sanvitto, V. G. Sala, R. Hivet, I. Carusotto, F. Pisanello, G. Leménager, R. Houdré, E. Giacobino, C. Ciuti, A. Bramati, *Science* **2011**, *332*, 1167.
[62] M. Sich, D. N. Krizhanovskii, M. S. Skolnick, A. V. Gorbach, R. Hartley, D. V. Skryabin, E. A. Cerda-Méndez, K. Biermann, R. Hey, P. V. Santos, *Nat. Photonics* **2012**, *6*, 50.
[63] G. Tosi, G. Christmann, N. G. Berloff, P. Tsotsis, T. Gao, Z. Hatzopoulos, P. G. Savvidis, J. J. Baumberg, *Nat. Phys.* **2012**, *8*, 190.
[64] E. Wertz, L. Ferrier, D. D. Solnyshkov, R. Johne, D. Sanvitto, A. Lemaître, I. Sagnes, R. Grousson, A. V. Kavokin, P. Senellart, G. Malpuech, J. Bloch, *Nat. Phys.* **2010**, *6*, 860.
[65] N. G. Berloff, M. Silva, K. Kalinin, A. Askitopoulos, J. D. Töpfer, P. Cilibrizzi, W. Langbein, P. G. Lagoudakis, *Nat. Mater.* **2017**, *16*, 1120.
[66] A. Kavokin, G. Malpuech, M. Glazov, *Phys. Rev. Lett.* **2005**, *95*, 136601.
[67] C. Leyder, M. Romanelli, K. J. Ph., E. Giacobino, T. C. H. Liew, M. M. Glazov, A. V. Kavokin, G. Malpuech, A. Bramati, *Nat. Phys.* **2007**, *3*, 628.
[68] T. Karzig, C.-E. Bardyn, N. H. Lindner, G. Refael, *Phys. Rev. X.* **2015**, *5*, 031001.
[69] M. Zhang, X. Wang, F. Song, R. Zhang, *Adv. Quantum Technol.* **2019**, *2*, 1800039.
[70] J. P. Karr, A. Baas, R. Houdré, E. Giacobino, *Phys. Rev. A* **2004**, *69*, 031802(R).
[71] T. Boulier, M. Bamba, A. Amo, C. Adrados, A. Lemaitre, E. Galopin, I. Sagnes, J. Bloch, C. Ciuti, E. Giacobino, A. Bramati, *Nat. Commun.* **2014**, *5*, 3260.
[72] H. Jabri, H. Eleuch, *J. Opt.* **2018**, *20*, 055201.
[73] A. Verger, C. Ciuti, I. Carusotto, *Phys. Rev. B* **2006**, *73*, 193306.
[74] F. Li, L. Orosz, O. Kamoun, S. Bouchoule, C. Brimont, P. Disseix, T. Guillet, X. Lafosse, M. Leroux, J. Leymarie, M. Mexis, M. Mihailovic, G. Patriarche, F. Réveret, D. Solnyshkov, J. Zuniga-Perez, G. Malpuech, *Phys. Rev. Lett.* **2013**, *110*, 196406.
[75] J. Kasprzak, D. D. Solnyshkov, R. André, L. S. Dang, G. Malpuech, *Phys. Rev. Lett.* **2008**, *101*, 146404.
[76] J. Levrat, R. Butté, E. Feltin, J.-F. Carlin, N. Grandjean, D. Solnyshkov, G. Malpuech, *Phys. Rev. B* **2010**, *81*, 125305.
[77] H. Eleuch, I. Rotter, *Phys. Rev. A* **2017**, *95*, 022117.
[78] H. Eleuch, I. Rotter, *Phys. Rev. A* **2016**, *93*, 042116.
[79] I. Rotter, *J. Phys. A: Math. Theor.* **2009**, *42*, 153001.
[80] I. Rotter, J. P. Bird, *Rep. Prog. Phys.* **2015**, *78*, 114001.
[81] M.-A. Miri, A. Alù, *Science* **2019**, *363*, eaar7709.
[82] T. Gao, E. Estrecho, K. Y. Bliokh, T. C. H. Liew, M. D. Fraser, S. Brodbeck, M. Kamp, C. Schneider, S. Höfling, Y. Yamamoto, F. Nori, Y. S. Kivshar, A. G. Truscott, R. G. Dall, E. A. Ostrovskaya, *Nature* **2015**, *526*, 554.
[83] C.-H. Wang, J. M. Taylor, *Phys. Rev. B* **2016**, *94*, 155437.
[84] V. N. Mantsevich, M. M. Glazov, *Phys. Rev. B* **2018**, *97*, 155308.
[85] S. R. K. Rodriguez, A. Amo, I. Sagnes, L. Le Gratiet, E. Galopin, A. Lemaître, J. Bloch, *Nat. Commun.* **2016**, *7*, 11887.
[86] F. Manni, Y. Léger, Y. G. Rubo, R. André, B. Deveaud, *Nat. Commun.* **2013**, *4*, 2590.
[87] M. Toledo-Solano, M. E. Mora-Ramos, A. Figueroa, Y. G. Rubo, *Phys. Rev. B* **2014**, *89*, 035308.
[88] R. Hivet, H. Flayac, D. D. Solnyshkov, D. Tanese, T. Boulier, D. Andreoli, E. Giacobino, J. Bloch, A. Bramati, G. Malpuech, A. Amo, *Nat. Phys.* **2012**, *8*, 724.
[89] S. Dufferwiel, F. Li, E. Cancellieri, L. Giriunas, A. A. P. Trichet, D. M. Whittaker, P. M. Walker, F. Fras, E. Clarke, J. M. Smith, M. S. Skolnick, D. N. Krizhanovskii, *Phys. Rev. Lett.* **2015**, *115*, 246401.
[90] V. G. Sala, D. D. Solnyshkov, I. Carusotto, T. Jacqmin, A. Lemaître, H. Terças, A. Nalitov, M. Abbarchi, E. Galopin, I. Sagnes, J. Bloch, G. Malpuech, A. Amo, *Phys. Rev. X.* **2015**, *5*, 011034.
[91] F. Li, E. Cancellieri, G. Buonaiuto, M. S. Skolnick, D. N. Krizhanovskii, D. M. Whittaker, *Phys. Rev. B* **2016**, *94*, 201301(R).
[92] M. Galbiati, L. Ferrier, D. D. Solnyshkov, D. Tanese, E. Wertz, A. Amo, M. Abbarchi, P. Senellart, I. Sagnes, A. Lemaître, G. Elisabeth, G. Malpuech, J. Bloch, *Phys. Rev. Lett.* **2012**, *108*, 126403.
[93] M. Bamba, A. Imamoğlu, I. Carusotto, C. Ciuti, *Phys. Rev. A* **2011**, *83*, 021802(R).
[94] X. W. Xu, Y. Li, *Phys. Rev. A* **2014**, *90*, 033809.
[95] L. Greuter, S. Starosielec, A. V. Kuhlmann, R. J. Warburton, *Phys. Rev. B* **2015**, *92*, 045302.
[96] A. Baas, J. P. Karr, H. Eleuch, E. Giacobino, *Phys. Rev. A* **2004**, *69*, 023809.
[97] D. N. Krizhanovskii, S. S. Gavrilov, A. P. D. Love, D. Sanvitto, N. A. Gippius, S. G. Tikhodeev, V. D. Kulakovskii, D. M. Whittaker, M. S. Skolnick, J. S. Roberts, *Phys. Rev. B* **2008**, *77*, 115336.

[98] A. A. Demenev, A. A. Shchekin, A. V. Larionov, S. S. Gavrilov, V. D. Kulakovskii, N. A. Gippius, S. G. Tikhodeev, *Phys. Rev. Lett.* **2008**, *101*, 136401.
[99] D. Sarkar, S. S. Gavrilov, M. Sich, J. H. Quilter, R. A. Bradley, N. A. Gippius, K. Guda, V. D. Kulakovskii, M. S. Skolnick, D. N. Krizhanovskii, *Phys. Rev. Lett.* **2010**, *105*, 216402.
[100] J. K. Chana, M. Sich, F. Fras, A. V. Gorbach, D. V. Skryabin, E. Cancellieri, E. A. Cerda-Méndez, K. Biermann, R. Hey, P. V. Santos, M. S. Skolnick, D. N. Krizhanovskii, *Phys. Rev. Lett.* **2015**, *115*, 256401.
[101] E. M. Kessler, G. Giedke, A. Imamoglu, S. F. Yelin, M. D. Lukin, J. I. Cirac, *Phys. Rev. A* **2012**, *86*, 012116.
[102] G. Muñoz-Matutano, A. Wood, M. Johnsson, X. Vidal, B. Q. Baragiola, A. Reinhard, A. Lemaître, J. Bloch, A. Amo, G. Nogues, B. Besga, M. Richard, T. Volz, *Nat. Mater.* **2019**, *18*, 213.
[103] A. Delteil, T. Fink, A. Schade, S. Höfling, C. Schneider, A. İmamoğlu, *Nat. Mater.* **2019**, *18*, 219.
[104] K. He, N. Kumar, L. Zhao, Z. Wang, K. F. Mak, H. Zhao, J. Shan, *Phys. Rev. Lett.* **2014**, *113*, 026803.
[105] A. Chernikov, T. C. Berkelbach, H. M. Hill, A. Rigosi, Y. Li, O. B. Aslan, D. R. Reichman, M. S. Hybertsen, T. F. Heinz, *Phys. Rev. Lett.* **2014**, *113*, 076802.
[106] M. M. Ugeda, A. J. Bradley, S.-F. Shi, H. Felipe, Y. Zhang, D. Y. Qiu, W. Ruan, S.-K. Mo, Z. Hussain, Z.-X. Shen, F. Wang, S. G. Louie, M. F. Crommie, *Nat. Mater.* **2014**, *13*, 1091.
[107] X. Liu, T. Galfsky, Z. Sun, F. Xia, E.-C. Lin, Y.-H. Lee, S. Kéna-Cohen, V. M. Menon, *Nat. Photonics* **2015**, *9*, 30.
[108] S. Schwarz, S. Dufferwiel, P. M. Walker, F. Withers, A. A. P. Trichet, M. Sich, F. Li, E. A. Chekhovich, D. N. Borisenko, N. N. Kolesnikov, K. S. Novoselov, M. S. Skolnick, J. M. Smith, D. N. Krizhanovskii, A. I. Tartakovskii, *Nano Lett.* **2014**, *14*, 7003.
[109] S. Dufferwiel, S. Schwarz, F. Withers, A. A. P. Trichet, F. Li, M. Sich, O. Del Pozo-Zamudio, C. Clark, A. Nalitov, D. D. Solnyshkov, G. Malpuech, K. S. Novoselov, J. M. Smith, M. S. Skolnick, D. N. Krizhanovskii, A. I. Tartakovskii, *Nat. Commun.* **2015**, *6*, 8579.
[110] L. C. Flatten, Z. He, D. M. Coles, A. A. P. Trichet, A. W. Powell, R. A. Taylor, J. H. Warner, J. M. Smith, *Sci. Rep.* **2016**, *6*, 33134.
[111] S. Dufferwiel, T. P. Lyons, D. D. Solnyshkov, A. A. P. Trichet, F. Withers, S. Schwarz, G. Malpuech, J. M. Smith, K. S. Novoselov, M. S. Skolnick, D. N. Krizhanovskii, A. I. Tartakovskii, *Nat. Photonics* **2017**, *11*, 497.
[112] M. Z. Maialle, E. A. de Andrada e Silva, L. J. Sham, *Phys. Rev. B* **1993**, *47*, 15776.
[113] M. M. Glazov, T. Amand, X. Marie, D. Lagarde, L. Bouet, B. Urbaszek, *Phys. Rev. B* **2014**, *89*, 201302(R).
[114] H. Yu, G.-B. Liu, P. Gong, X. Xu, W. Yao, *Nat. Commun.* **2014**, *5*, 3876.
[115] S. Dufferwiel, T. P. Lyons, D. D. Solnyshkov, A. A. P. Trichet, A. Catanzaro, F. Withers, G. Malpuech, J. M. Smith, K. S. Novoselov, M. S. Skolnick, D. N. Krizhanovskii, A. I. Tartakovskii, *Nat. Commun.* **2018**, *9*, 4794.
[116] J. T. Devreese, in *Encyclopedia of Physics*, Vol. *2* (Eds: R. G. Lerner, G. L. Trigg), Wiley-VCH, Weinheim, Germany **2005**.
[117] M. Sidler, P. Back, O. Cotlet, A. Srivastava, T. Fink, M. Kroner, E. Demler, A. Imamoglu, *Nat. Phys.* **2017**, *13*, 255.
[118] D. G. Lidzey, D. D. C. Bradley, M. S. Skolnick, T. Virgili, S. Walker, D. M. Whittaker, *Nature* **1998**, *395*, 53.
[119] J. R. Tischler, M. S. Bradley, V. Bulović, J. H. Song, A. Nurmikko, *Phys. Rev. Lett.* **2005**, *95*, 036401.
[120] K. S. Daskalakis, S. A. Maier, R. Murray, S. Kéna-Cohen, *Nat. Mater.* **2014**, *13*, 271.
[121] J. D. Plumhof, T. Stöferle, L. Mai, U. Scherf, R. F. Mahrt, *Nat. Mater.* **2014**, *13*, 247.
[122] D. Urbonas, T. Stöferle, F. Scafirimuto, U. Scherf, R. F. Mahrt, *ACS Photonics* **2016**, *3*, 1542.
[123] F. Scafirimuto, D. Urbonas, U. Scherf, R. F. Mahrt, T. Stöferle, *ACS Photonics* **2018**, *5*, 85.
[124] S. Betzold, S. Herbst, A. A. P. Trichet, J. M. Smith, F. Würthner, S. Höfling, C. P. Dietrich, *ACS Photonics* **2018**, *5*, 90.
[125] R. T. Grant, R. Jayaprakash, D. M. Coles, A. Musser, L. S. De, S. Idw, G. A. Turnbull, J. Clark, D. G. Lidzey, *Opt. Express* **2018**, *26*, 3320.
[126] R. Pan, U. Retzer, T. Werblinski, M. N. Slipchenko, T. R. Meyer, L. Zigan, S. Will, *Opt. Lett.* **2018**, *43*, 1191.
[127] D. M. Coles, A. A. P. Trichet, P. R. Dolan, R. A. Taylor, C. Vallance, J. M. Smith, *Laser Photonics Rev.* **2015**, *9*, 538.
[128] J. Marelic, L. F. Zajiczek, H. J. Hesten, K. H. Leung, E. Y X Ong, F. Mintert, R. A. Nyman, *New J. Phys.* **2016**, *18*, 103012.
[129] J. Klaers, J. Schmitt, F. Vewinger, M. Weitz, *Nature* **2010**, *468*, 545.
[130] J. Klaers, F. Vewinger, M. Weitz, *Nat. Phys.* **2010**, *6*, 512.
[131] J. Marelic, R. A. Nyman, *Phys. Rev. A* **2015**, *91*, 033813.
[132] J. Marelic, B. T. Walker, R. A. Nyman, *Phys. Rev. A* **2016**, *94*, 063812.
[133] B. T. Walker, L. C. Flatten, H. J. Hesten, F. Mintert, D. Hunger, A. A. P. Trichet, J. M. Smith, R. A. Nyman, *Nat. Phys.* **2018**, *14*, 1173.
[134] F. Lenzini, N. Gruhler, N. Walter, W. H. P. Pernice, *Adv. Quantum Technol.* **2018**, *1*, 1800061.
[135] S. Hepp, M. Jetter, S. L. Portalupi, P. Michler, *Adv. Quantum Technol.* **2019**, 1900020.
[136] P. Lodahl, S. Mahmoodian, S. Stobbe, *Rev. Mod. Phys.* **2015**, *87*, 347.
[137] F. Liu, A. J. Brash, J. O'Hara, L. M. P. P. Martins, C. L. Phillips, R. J. Coles, B. Royall, E. Clarke, C. Bentham, N. Prtljaga, I. E. Itskevich, L. R. Wilson, M. S. Skolnick, A. M. Fox, *Nat. Nanotechnol.* **2018**, *13*, 835.
[138] H. Wang, H. Hu, T. H. Chung, J. Qin, X. X. Yang, J. P. Li, R. Z. Liu, H. S. Zhong, Y. M. He, X. Ding, Y. H. Deng, Q. Dai, Y. H. Huo, S. Hofling, C. Y. Lu, J. W. Pan, *Phys. Rev. Lett.* **2019**, *122*, 113602.
[139] P. Senellart, G. Solomon, A. White, *Nat. Nanotechnol.* **2017**, *12*, 1026.
[140] A. Imamoglu, D. D. Awschalom, G. Burkard, D. P. DiVincenzo, D. Loss, M. Sherwin, A. Small, *Phys. Rev. Lett.* **1999**, *83*, 4204.
[141] N. Yokoshi, H. Imamura, H. Kosaka, *Phys. Rev. B* **2013**, *88*, 155321.
[142] N. S. Maslova, P. I. Arseyev, V. N. Mantsevich, *Phys. Rev. E* **2018**, *97*, 022135.
[143] A. Badolato, K. Hennessy, M. Atatüre, J. Dreiser, E. Hu, P. M. Petroff, A. Imamoğlu, *Science* **2005**, *308*, 1158.
[144] A. Dousse, L. Lanco, J. Suffczyński, E. Semenova, A. Miard, A. Lemaître, I. Sagnes, C. Roblin, J. Bloch, P. Senellart, *Phys. Rev. Lett.* **2008**, *101*, 267404.
[145] S. Strauf, N. G. Stoltz, M. T. Rakher, L. A. Coldren, P. M. Petroff, D. Bouwmeester, *Nat. Photonics* **2007**, *1*, 704.
[146] C. Kistner, T. Heindel, C. Schneider, A. Rahimi-Iman, S. Reitzenstein, S. Höfling, A. Forchel, *Opt. Express* **2008**, *16*, 15006.
[147] A. Laucht, F. Hofbauer, N. Hauke, J. Angele, S. Stobbe, M. Kaniber, G. Böhm, P. Lodahl, M.-C. Amann, J. J. Finley, *New J. Phys.* **2009**, *11*, 023034.
[148] L. Greuter, D. Najer, A. V. Kuhlmann, S. Valentin, A. Ludwig, A. D. Wieck, S. Starosielec, R. J. Warburton, *J. Appl. Phys.* **2015**, *118*, 075705.
[149] Z. Di, H. V. Jones, P. R. Dolan, S. M. Fairclough, M. B. Wincott, J. Fill, G. M. Hughes, J. M. Smith, *New J. Phys.* **2012**, *14*, 103048.
[150] R. K. Patel, A. A. P. Trichet, D. M. Coles, P. R. Dolan, S. M. Fairclough, M. A. Leontiadou, S. C. E. Tsang, D. J. Binks, E. Jang, H. Jang, R. A. Taylor, J. M. Smith, *Adv. Opt. Mater.* **2016**, *4*, 285.
[151] G. Balasubramanian, P. Neumann, D. Twitchen, M. Markham, R. Kolesov, N. Mizuochi, J. Isoya, J. Achard, J. Beck, J. Tissler, V. Jacques, P. R. Hemmer, F. Jelezko, J. Wrachtrup, *Nat. Mater.* **2009**, *8*, 383.
[152] C. Kurtsiefer, S. Mayer, P. Zarda, H. Weinfurter, *Phys. Rev. Lett.* **2000**, *85*, 290.

[153] J. Wolters, A. W. Schell, G. Kewes, N. Nüsse, M. Schoengen, H. Döscher, T. Hannappel, B. Löchel, M. Barth, O. Benson, *Appl. Phys. Lett.* **2010**, *97*, 141108.
[154] A. Faraon, P. E. Barclay, C. Santori, K.-M. C. Fu, R. G. Beausoleil, *Nat. Photonics* **2011**, *5*, 301.
[155] C. Santori, P. E. Barclay, K.-M. C. Fu, R. G. Beausoleil, S. Spillane, M. Fisch, *Nanotechnology* **2010**, *21*, 274008.
[156] S. Johnson, P. R. Dolan, T. Grange, A. A. P. Trichet, G. Hornecker, Y. C. Chen, L. Weng, G. M. Hughes, A. A. R. Watt, A. Auffèves, J. M. Smith, *New J. Phys.* **2015**, *17*, 122003.
[157] P. R. Dolan, S. Adekanye, A. A. P. Trichet, S. Johnson, L. C. Flatten, Y. C. Chen, L. Weng, D. Hunger, H. C. Chang, S. Castelletto, J. M. Smith, *Opt. Express* **2018**, *26*, 7056.
[158] H. Kaupp, T. Hümmer, M. Mader, B. Schlederer, J. Benedikter, P. Haeusser, H. C. Chang, H. Fedder, T. W. Hänsch, D. Hunger, *Phys. Rev. Appl.* **2016**, *6*, 054010.
[159] D. Riedel, I. Söllner, B. J. Shields, S. Starosielec, P. Appel, E. Neu, P. Maletinsky, R. J. Warburton, *Phys. Rev. X* **2017**, *7*, 031040.
[160] S. Bogdanovic, M. S. Z. Liddy, S. B. V. Dam, L. C. Coenen, T. Fink, M. Loncar, R. Hanson, *APL Photonics* **2017**, *2*, 126101.
[161] R. Chikkaraddy, B. de Nijs, F. Benz, S. J. Barrow, O. A. Scherman, E. Rosta, A. Demetriadou, P. Fox, O. Hess, J. J. Baumberg, *Nature* **2016**, *535*, 127.
[162] R. Liu, Z.-K. Zhou, Y.-C. Yu, T. Zhang, H. Wang, G. Liu, Y. Wei, H. Chen, X.-H. Wang, *Phys. Rev. Lett.* **2017**, *118*, 237401.
[163] C. Toninelli, Y. Delley, T. Stöferle, A. Renn, S. Götzinger, V. Sandoghdar, *Appl. Phys. Lett.* **2010**, *97*, 021107.
[164] D. Wang, H. Kelkar, D. Martin-Cano, T. Utikal, S. Götzinger, V. Sandoghdar, *Phys. Rev. X* **2017**, *7*, 021014.
[165] S. Tang, B. Li, Y. Xiao, *Physics* **2019**, *48*, 137.
[166] F. Vollmer, L. Yang, *Nanophotonics* **2012**, *1*, 267.
[167] Y. Zhi, X. C. Yu, Q. Gong, L. Yang, Y. F. Xiao, *Adv. Mater.* **2017**, *29*, 1604920.
[168] E. Kim, M. D. Baaske, F. Vollmer, *Lab Chip* **2017**, *17*, 1190.
[169] A. A. P. Trichet, J. Foster, N. E. Omori, D. James, P. R. Dolan, G. M. Hughes, C. Vallance, J. M. Smith, *Lab Chip* **2014**, *14*, 4244.
[170] J. G. Velez, A. Muller, *Appl. Phys. Lett.* **2018**, *112*, 041107.
[171] R. M. Heath, M. G. Tanner, R. A. Kirkwood, S. Miki, R. J. Warburton, R. H. Hadfield, *J. Appl. Phys.* **2016**, *120*, 113101.
[172] B. Gurlek, V. Sandoghdar, D. Martín-Cano, *ACS Photonics* **2018**, *5*, 456.
[173] P. Peng, Y.-C. Liu, D. Xu, Q.-T. Cao, G. Lu, Q. Gong, Y.-F. Xiao, *Phys. Rev. Lett.* **2017**, *119*, 233901.
[174] Y.-F. Xiao, Y.-C. Liu, B.-B. Li, Y.-L. Chen, Y. Li, Q. Gong, *Phys. Rev. A* **2012**, *85*, 031805(R).
[175] Y. He, X. Ding, Z.-E. Su, H.-L. Huang, J. Qin, C. Wang, S. Unsleber, C. Chen, H. Wang, Y.-M. He, X.-L. Wang, W.-J. Zhang, S.-J. Chen, C. Schneider, M. Kamp, L.-X. You, Z. Wang, S. Hofling, C.-Y. Lu, J.-W. Pan, *Phys. Rev. Lett.* **2017**, *118*, 190501.
[176] H. Wang, Y. He, Y.-H. Li, Z.-E. Su, B. Li, H.-L. Huang, X. Ding, M.-C. Chen, C. Liu, J. Qin, J.-P. Li, Y.-M. He, C. Schneider, M. Kamp, C.-Z. Peng, S. Höfling, C.-Y. Lu, J.-W. Pan, *Nat. Photonics* **2017**, *11*, 361.
[177] A. Reinhard, T. Volz, M. Winger, A. Badolato, K. J. Hennessy, E. L. Hu, A. Imamoğlu, *Nat. Photonics* **2012**, *6*, 93.
[178] C. Qian, S. Wu, F. Song, K. Peng, X. Xie, J. Yang, S. Xiao, M. J. Steer, I. G. Thayne, C. Tang, Z. Zuo, K. Jin, C. Gu, X. Xu, *Phys. Rev. Lett.* **2018**, *120*, 213901.
[179] E. Nagali, F. Sciarrino, F. D. Martini, L. Marrucci, B. Piccirillo, E. Karimi, E. Santamato, *Phys. Rev. Lett.* **2009**, *103*, 013601.
[180] R. Fickler, R. Lapkiewicz, M. Huber, M. P. J. Lavery, M. J. Padgett, A. Zeilinger, *Nat. Commun.* **2014**, *5*, 4502.
[181] Y. Chen, J. Gao, Z.-Q. Jiao, K. Sun, W.-G. Shen, L.-F. Qiao, H. Tang, X.-F. Lin, X.-M. Jin, *Phys. Rev. Lett.* **2018**, *121*, 233602.
[182] T. C. H. Liew, M. M. Glazov, K. V. Kavokin, I. A. Shelykh, M. A. Kaliteevski, A. V. Kavokin, *Phys. Rev. Lett.* **2013**, *110*, 047402.
[183] E. A. Cerda-Méndez, D. N. Krizhanovskii, M. Wouters, R. Bradley, K. Biermann, K. Guda, R. Hey, P. V. Santos, D. Sarkar, M. S. Skolnick, *Phys. Rev. Lett.* **2010**, *105*, 116402.
[184] E. A. Cerda-Méndez, D. Sarkar, D. N. Krizhanovskii, S. S. Gavrilov, K. Biermann, M. S. Skolnick, P. V. Santos, *Phys. Rev. Lett.* **2013**, *111*, 146401.